SLAC-PUB-2136
June 1978
(T/E)

QUARK AND LEPTON COUPLINGS IN THE WEAK INTERACTIONS*

L. F. Abbott and R. Michael Barnett
Stanford Linear Accelerator Center
Stanford University, Stanford, California 94305

ABSTRACT

We present a comprehensive study of the weak neutral-current interactions of u and d quarks and of the electron. A model-independent analysis using data from deep-inelastic, inclusive-pion, elastic and exclusive-pion neutrino processes provides a unique determination of the u and d quark couplings. For electron couplings, neutrino-electron-scattering, atomic-parity-violation and new polarized-electron-scattering data are discussed. With the assumption of a single Z^o boson, we show that the electron couplings are almost uniquely determined. The predictions of the Weinberg-Salam model (for $\sin^2\theta_W = 0.20\text{-}0.30$) are in remarkably good agreement with our results.

(Submitted to Phys. Rev. D)

*Work supported by the Department of Energy

I. INTRODUCTION

In the past few years sufficient progress has been made in the experimental study of weak interactions to permit a unique determination of the neutral-current couplings of u and d quarks[1] and to provide considerable information on the neutral-current couplings of the electron as well. We present here a comprehensive analysis of neutral-current interactions and their implications for the weak couplings of both quarks and leptons. Our results are compared with the predictions of several gauge theories of weak and electromagnetic interactions and in particular, with the $SU(2)\times U(1)$ model of Weinberg and Salam.[2] Our procedure is to "invert" the results of a given experiment and indicate regions of the quark or electron coupling-constant space which are allowed by the data. The area which is overlapped by all of the allowed regions from the various experiments considered then provides a determination of these couplings. Ninety percent confidence limits are used for all experimental results and theoretical uncertainties are taken into account when they are significant.

In Section II, we present a detailed account of our unique determination of the u and d quark neutral-current couplings. This determination is based on the analysis of data from deep-inelastic neutrino scattering,[3] neutrino-induced inclusive pion production,[4] elastic neutrino-proton scattering,[5] and neutrino-induced exclusive pion production.[6] New elastic-scattering data[5] and new high-energy inclusive-pion data[7] are used to strengthen our conclusions on the uniqueness of the quark-coupling determination which we have previously reported.[1]

The neutral-current couplings of the electron are discussed in Section III. Data[8] from muon-neutrino(ν_μ), muon-antineutrino($\bar{\nu}_\mu$) and electron-antineutrino($\bar{\nu}_e$) scattering off electrons are considered. Our determination of the quark couplings along with the assumption of one Z^o boson allows us to use parity-violation experiments[9,10] to further restrict the allowed values of electron couplings. We discuss results on parity violation for transitions in bismuth atoms.[9] Most importantly, we present an analysis of data from a polarized-electron scattering experiment[10] performed recently at SLAC. If we assume that only one Z^o boson exists, these SLAC results along with the data from neutrino-electron scattering experiments provide an almost unique determination of the electron couplings of the weak-neutral current.

Our results on both quark and electron couplings are in excellent agreement with predictions of the Weinberg-Salam (WS) model[2] with the Glashow-Iliopoulos-Maiani (GIM) mechanism[11] incorporated. Since our allowed range of coupling values is extremely restrictive, we view such agreement as a striking success for this model.

II. QUARK COUPLINGS

We assume that the neutral-current interactions of neutrinos with u and d quarks occur through the effective interaction Lagrangian

$$\mathscr{L} = \frac{G}{\sqrt{2}} \bar{\nu}\gamma^\mu(1+\gamma_5)\nu \left[u_L\bar{u}\gamma_\mu(1+\gamma_5)u + u_R\bar{u}\gamma_\mu(1-\gamma_5)u + d_L\bar{d}\gamma_\mu(1+\gamma_5)d + d_R\bar{d}\gamma_\mu(1-\gamma_5)d\right] \quad . \tag{2.1}$$

Our problem then is to determine the values of the quark coupling constants u_L, d_L, u_R, and d_R appearing in the above Lagrangian by using data from deep-inelastic,[3] pion-inclusive,[4] elastic,[5] and pion-exclusive[6] processes. Note that the use of this effective Lagrangian does not restrict us to any particular types of gauge models. In fact, it is applicable to any model with vector and axial-vector currents having the usual properties under charge conjugation. The quark coupling constants may represent the effects of summing over more than one massive, neutral vector-boson. We ignore the small effects caused by the neutral currents of s, c and other heavy quarks. Finally, the overall sign of the Lagrangian (2.1) is always ambiguous in neutrino interactions, so we will choose a sign convention by requiring u_L to be positive (with no loss in generality).

A. Deep-Inelastic Scattering

The data from deep-inelastic neutrino ($\nu N \to \nu X$, where $X \equiv$ anything) scattering experiments[3] are analysed using a standard parton model calculation.[12] For this discussion, we will ignore the effects of antiquarks in the nucleon. The complete cross-section formulas including the effects of antiquarks and of an experimental cut on the total hadronic energy are given in Appendix A. Actually, our results are fairly insensitive to the presence of s quarks and to variations in the antiquark to quark ratio in the range of 0% to 20%. A ratio of 16% was used in our calculations.[13] Ignoring antiquarks and QCD corrections, the cross-sections for neutral-current (NC) and for charged-current (CC) deep-inelastic scattering of neutrinos off an isoscalar target are

$$\sigma_\nu^{NC} = \frac{G^2 mE}{\pi} \int dx\, F(x) \left[(u_L^2+d_L^2) + \frac{1}{3}\,(u_R^2 + d_R^2)\right] \qquad (2.2)$$

$$\sigma_{\nu}^{CC} = \frac{G^2 mE}{\pi} \int dx\ F(x)\ [1] \tag{2.3}$$

and for antineutrinos

$$\sigma_{\bar{\nu}}^{NC} = \frac{G^2 mE}{\pi} \int dx\ F(x) \left[\frac{1}{3}(u_L^2+d_L^2) + (u_R^2+d_R^2)\right] \tag{2.4}$$

$$\sigma_{\bar{\nu}}^{CC} = \frac{G^2 mE}{\pi} \int dx\ F(x) \left[\frac{1}{3}\right] \tag{2.5}$$

G is the usual Fermi coupling constant ($G \approx 10^{-5}/m^2$), m is the nucleon mass and F(x) is a measure of the momentum distribution of quarks inside the nucleon and is equal to νW_2. Taking ratios we find

$$R_{\nu} = \frac{\sigma_{\nu}^{NC}}{\sigma_{\nu}^{CC}} = \frac{(u_L^2+d_L^2) + \frac{1}{3}(u_R^2+d_R^2)}{(1)} \tag{2.6}$$

and

$$R_{\bar{\nu}} = \frac{\sigma_{\bar{\nu}}^{NC}}{\sigma_{\bar{\nu}}^{CC}} = \frac{\frac{1}{3}(u_L^2+d_L^2) + (u_R^2+d_R^2)}{\frac{1}{3}} \tag{2.7}$$

Thus, a knowledge of R_{ν} and $R_{\bar{\nu}}$ determines values of $(u_L^2+d_L^2)$ and $(u_R^2+d_R^2)$ which give the radii of circles in plots of u_L vs. d_L and u_R vs. d_R.

Using the results of the CERN-Dortmund-Heidelberg-Saclay (CDHS) group[3] ($R_{\nu}=0.295\pm0.01$ and $R_{\bar{\nu}}=0.34\pm0.03$), the values of the radii in the left and right coupling-constant planes allowed at the 90% confidence level are shown in Fig. 1. Note that we have restricted ourselves to the upper half of the left-coupling plane in keeping with our sign convention $u_L \geq 0$. As Fig. 1 shows, the deep-inelastic data give a fairly good determination of the allowed radii, especially in the left-coupling plane, but they give no information on the allowed angular ranges around these radii. This is because in an inclusive deep-inelastic scattering

experiment off an isoscalar target one has no knowledge about what type of quark is being struck and so one obtains no information about the isospin structure of the neutral-current.

B. Inclusive Pion Production

In inclusive pion production ($\nu N \rightarrow \nu \pi X$), the charge of a leading pion can be used as an indicator of the identity of the struck quark.[14] To insure that a given pion is a decay product of the struck quark, one requires that the fraction z of the total hadronic energy carried by this pion be greater than some minimum value z_1. It may also be necessary to restrict ourselves to z less than some maximum value z_2 in order to avoid resonances which are not included in the parton model. Pion-inclusive data can then be used to obtain some isospin information about the neutral current which is not provided by the deep-inelastic results.

The analysis of pion-inclusive data is very similar to the analysis of deep-inelastic data except that a factor must be inserted to account for the probability of a pion being present in the final state. This factor is the quark fragmentation function $D_q^{\pi}(z)$ which gives the probability that a pion of a given charge with fraction z of the total hadronic energy will be produced by a quark q. The number of pions produced in the range $z_1 \leq z \leq z_2$ is then obtained by multiplying the cross-section for scattering off a certain quark by the probability for that quark to produce a given pion, summing over quark types, and integrating over z. Ignoring antiquarks and experimental cuts this gives the following expressions for π^+ to π^- multiplicity ratios:

$$\left(\frac{N_{\pi^+}}{N_{\pi^-}}\right)_{\nu} = \frac{(u_L^2 + \frac{1}{3}u_R^2)\int_{z_1}^{z_2} dz\, D_u^{\pi^+} + (d_L^2 + \frac{1}{3}d_R^2)\int_{z_1}^{z_2} dz\, D_d^{\pi^+}}{(u_L^2 + \frac{1}{3}u_R^2)\int_{z_1}^{z_2} dz\, D_u^{\pi^-} + (d_L^2 + \frac{1}{3}d_R^2)\int_{z_1}^{z_2} dz\, D_d^{\pi^-}} \tag{2.8a}$$

$$\left(\frac{N_{\pi^+}}{N_{\pi^-}}\right)_{\bar{\nu}} = \frac{(u_R^2 + \frac{1}{3}u_L^2)\int_{z_1}^{z_2} dz\, D_u^{\pi^+} + (d_R^2 + \frac{1}{3}d_L^2)\int_{z_1}^{z_2} dz\, D_d^{\pi^+}}{(u_R^2 + \frac{1}{3}u_L^2)\int_{z_1}^{z_2} dz\, D_u^{\pi^-} + (d_R^2 + \frac{1}{3}d_L^2)\int_{z_1}^{z_2} dz\, D_d^{\pi^-}} \tag{2.8b}$$

The complete expressions including the effects of antiquarks and a hadronic energy cut are given in Appendix B. The quark fragmentation functions satisfy the isospin relations

$$D_u^{\pi^+} = D_d^{\pi^-} \tag{2.9}$$

and

$$D_u^{\pi^-} = D_d^{\pi^+} \tag{2.10}$$

Thus, Eqs. (2.8a) and (2.8b) only depend on the fragmentation functions through the ratio

$$\eta \equiv \frac{\int_{z_1}^{z_2} dz\, D_u^{\pi^+}}{\int_{z_1}^{z_2} dz\, D_u^{\pi^-}} \tag{2.11}$$

This ratio has been measured[15] in both electroproduction and charged-current experiments to be $\eta = 2.8 \pm 0.7$ for $z_1 = 0.3$ and $z_2 = 0.7$. Equations (2.8a) and (2.8b) can be rewritten simply in terms of η as

$$\left(\frac{N_{\pi+}}{N_{\pi-}}\right)_{\nu} = -\frac{(u_L^2 + \frac{1}{3}u_R^2)\eta + (d_L^2 + \frac{1}{3}d_R^2)}{(u_L^2 + \frac{1}{3}u_R^2) + (d_L^2 + \frac{1}{3}d_R^2)\eta} \tag{2.12a}$$

$$\left(\frac{N_{\pi+}}{N_{\pi-}}\right)_{\bar{\nu}} = \frac{(u_R^2 + \frac{1}{3}u_L^2)\eta + (d_R^2 + \frac{1}{3}d_L^2)}{(u_R^2 + \frac{1}{3}u_L^2) + (d_R^2 + \frac{1}{3}d_L^2)\eta} \tag{2.12b}$$

Data are available on these pion multiplicity ratios from Gargamelle at the CERN PS.[4] The ratios found are $(N_{\pi+}/N_{\pi-})_{\nu} = 0.77\pm0.14$ and $(N_{\pi+}/N_{\pi-})_{\bar{\nu}} = 1.64\pm0.36$ with $z_1=0.3$, $z_2=0.7$ and a hadronic energy cut $E_{had} > 1$ GeV. An antiquark to quark ratio of 5% was used in our analysis of these low-energy data. At the 90% confidence level the allowed coupling constant values are indicated by the regions shaded with dots in Fig. 1. The two allowed regions in the left-coupling plane and the two in the right-coupling plane combine to give four allowed combinations, as noted by Sehgal[14] (and discussed by others[1,16]).

In order to distinguish between these four regions, we will next consider exclusive scattering data. These provide correlations between left and right coupling values which cannot be displayed in a plot like that of Fig. 1. To display such correlations, we consider fixed radii in the left and right coupling constant planes and parameterize the quark couplings in terms of the angles

$$\theta_L = \arctan\,(u_L/d_L) \tag{2.13}$$

$$\theta_R = \arctan\,(u_R/d_R) \quad . \tag{2.14}$$

This is done in Figs. 2–4 where the radius in the left-coupling plane was chosen at the center of the annulus allowed by deep-inelastic data (at $\hat{0}.53$); and the radius in the right-coupling plane was chosen to span the allowed annulus taking the values 0.22, 0.175, and 0.13 in Figs. 2, 3, and 4 respectively. (Variations in the radius for the left-coupling plane within the allowed annulus produce little effect and so are not shown.) Note that, in keeping with our sign convention for u_L, θ_L goes only from 0° to 180° whereas θ_R ranges from 0° to 360°.

The four regions allowed by this pion-inclusive data are those inside the four ellipses in Figs. 2 and 3. There are no allowed angles for the smallest right-coupling radius depicted in Fig. 4. The region centered at $\theta_L=140^\circ$ and $\theta_R=270^\circ$ will be referred to as A; that at $\theta_L=140^\circ$, $\theta_R=90^\circ$ as region B; that at $\theta_L=40^\circ$, $\theta_R=90^\circ$ as C; and that at $\theta_L=40^\circ$, $\theta_R=270^\circ$ as D. Regions A and B give a strongly isovector neutral current while C and D give a strongly isoscalar result. Likewise, A and D are axial-vector dominated while B and C are vector dominated.

Unfortunately, the data cited above[4] were taken at fairly low energies so the extensive use of the parton model in the pion-inclusive analysis might be questioned. It is therefore of great importance to obtain values of the pion multiplicity ratios at high energies. Data are available from Fermilab on charged-particle multiplicites from high-energy neutral-current interactions for neutrinos[7] (but not yet for antineutrinos). We have corrected (using SLAC data)[17] these data for protons and kaons which are present along with the pions and have obtained results in excellent agreement with those presented above. We find regions somewhat larger than the ellipses shown in Figs. 2 and 3, but which almost entirely

overlap those ellipses. With these high-energy data the right-hand boundaries (in Fig. 2) of ellipses A and B are moved from $\theta_L \approx 151^o$ to 148^o and the left-hand boundaries of C and D from $\theta_L \approx 29^o$ to 32^o. In addition, smaller radii (in Fig. 1) in the right-coupling plane are allowed. This will be of interest later. Except for these small discrepancies, these high-energy results[7] seem to be in excellent agreement with those of the lower-energy data.[4]

C. Elastic Scattering

The cross-section for elastic neutrino-proton scattering[18] is given in Appendix C. It is written in terms of the vector and axial-vector form-factors of the neutral current between proton states,

$$\langle p'|J_\mu^{NC}|p\rangle = \bar{u}(p')\left[\gamma_\mu F_1 + \frac{i\,\sigma_{\mu\nu}q^\nu}{2m} F_2 + \gamma_5\gamma_\mu F_A\right]u(p) \qquad (2.15)$$

These form-factors can be related to the quark coupling constants through an isospin decomposition,

$$F_i = (u_L - d_L + u_R - d_R)\, F_i^{I=1} + 3(u_L + d_L + u_R + d_R)\, F_i^{I=0} \quad (i=1,2) \qquad (2.16)$$

and

$$F_A = (u_L - d_L - u_R + d_R)F_A^{I=1} + \frac{3}{5}(u_L + d_L - u_R - d_R)F_A^{I=0} \qquad (2.17)$$

The factors of 3 and 3/5 between the isovector and isoscalar parts are obtained by considering the isospin structure of the SU(6) wavefunction of the nucleon.[19] The vector form-factors are related by CVC to the electromagnetic form-factors of the neutron and proton,

$$F_i^{I=1} = F_i^p - F_i^n \qquad (i=1,2) \qquad (2.18)$$

and

$$F_i^{I=0} = F_i^p + F_i^n \qquad (i=1,2) \tag{2.19}$$

The isovector, axial form-factor is measured in charged-current reactions and is

$$F_A^{I=1} = \frac{1.23}{\left(1 + \frac{Q^2}{m_A^2}\right)^2} \tag{2.20}$$

where $m_A^2 \approx .79\ \text{GeV}^2$. (Our results are not sensitive to variations of m_A within a reasonable range.) For the isoscalar axial form-factor we make the assumption

$$F_A^{I=0} = F_A^{I=1} \tag{2.21}$$

For regions A and B, the contribution of the isoscalar axial form-factor is fairly small.

The results of the Harvard-Pennsylvania-Wisconsin (HPW) group[5] are given in terms of ratios of neutral-current to charged-current elastic cross-sections. These ratios are $R_\nu = 0.11 \pm 0.02$ and $R_{\bar{\nu}} = 0.20 \pm 0.05$ for the range $0.4 \leq Q^2 \leq 0.9$. In using this data we have increased these statistical errors to account for possible systematic errors and theoretical uncertainties. At the 90% confidence level the allowed angular regions for the various radii are indicated in Figs. 2–4 by the areas shaded with lines and contained by dotted curves.

Region C which was allowed by the pion-inclusive data is now completely eliminated by these elastic scattering results. Region B is virtually eliminated as well; the only surviving part of region B is the edge right at $\theta_L = 150^\circ$ shown in Fig. 2. Recall, however, that this is precisely the edge which was eliminated by considering the high-energy pion-inclusive data.[7] Remaining are large portions of region D and all of region A.

Roughly speaking, the regions allowed by the elastic scattering results consist of two bands, one giving a predominantly isoscalar neutral-current and the other a largely isovector current. This type of isoscalar-isovector ambiguity can be resolved easily by exclusive pion production experiments because of the $\Delta(1232)$ resonance which acts as a probe of the isovector strength of the neutral current.[20]

D. Exclusive Pion Production

Exclusive pion production ($\nu N \to \nu N\pi$) data are analysed[1,21] using the pion production model developed by Adler.[22-24] This model is superior to all other pion-production models; it includes non-resonant production, incorporates excitation of the $\Delta(1232)$ resonance, and satisfies current algebra relations. It has been shown to be in good agreement with results from electro-production and charged-current production experiments.

We present here an outline of the general features of the model. Further details are presented in Appendix D. One begins with the Born amplitudes[22] coming from the diagrams of Fig. 5. These are written in terms of the nucleon form-factors F_1, F_2 and F_A discussed in Sec. II C; the pion form-factor (coming from Fig. 5c); and g_r, the pion-nucleon coupling constant. Two important corrections to these Born terms are then applied.

The first of these comes from current algebra which allows us to express pion-production amplitudes in the soft-pion limit in terms of nucleon-nucleon matrix elements.[23] This gives expressions similar to the Born amplitudes except that the pseudoscalar pion-nucleon coupling of Fig. 5 is replaced by an axial-vector coupling which then implies that certain vertex corrections must be made to the Born amplitudes. In

addition, there are new terms coming from an equal-time commutator in the current algebra relations.

The Born amplitudes with current algebra corrections included are then broken up into multipoles of specified spin and isospin. Those multipoles with the $J = 3/2$, $I = 3/2$ quantum numbers of the $\Delta(1232)$ resonance must then be corrected for resonant rescattering in the final state. This is done by multiplying them by a phase $e^{i\delta_R}$ and an enhancement factor.[22] It is crucial to keep the non-resonant (including $I = 1/2$) multipoles as well since both our analysis and the data show that they are important.[25]

To avoid other (higher mass) resonances and for consistency with the soft-pion assumption, it is necessary to require that the invariant mass of the final-state pion-nucleon system be less than 1.4 GeV. Unfortunately, the data are not available with this cut, and for channels with a final-state neutron it is, of course, difficult to determine this mass. However, the relevance of the cut to our conclusions is minimal because: 1) most data are below the 1.4 GeV cut, 2) ratios of cross-sections are always used, 3) application of the cut to the limited experimental mass plots available indicate a strengthening of our conclusions, and 4) the model predictions are assumed to be valid only within 30% and the data are taken at the 90% confidence level.[26]

Results are available from Gargamelle[6] for the following cross-section ratios:

$$R^{\nu}_{p\pi^0} \equiv \frac{\sigma(\nu p \to \nu p \pi^0)}{\sigma(\nu n \to \mu^- p \pi^0)} \tag{2.22}$$

$$R^{\nu}_{n\pi^o} \equiv \frac{\sigma(\nu n \to \nu n \pi^o)}{\sigma(\nu n \to \mu^- p \pi^o)} \tag{2.23}$$

$$R^{\nu}_{p\pi^-} \equiv \frac{\sigma(\nu n \to \nu p \pi^-)}{\sigma(\nu n \to \mu^- p \pi^o)} \tag{2.24}$$

$$R^{\nu}_{n\pi^+} \equiv \frac{\sigma(\nu p \to \nu n \pi^+)}{\sigma(\nu n \to \mu^- p \pi^o)} \tag{2.25}$$

$$\tilde{R}^{\bar{\nu}}_{0} \equiv \frac{1.22\ \sigma(\bar{\nu} p \to \bar{\nu} p \pi^o) + \sigma(\bar{\nu} n \to \bar{\nu} n \pi^o)}{2(1.22)\sigma(\bar{\nu} p \to \mu^+ n \pi^o)} \tag{2.26}$$

and

$$R^{\bar{\nu}}_{p\pi^-} \equiv \frac{\sigma(\bar{\nu} n \to \bar{\nu} p \pi^-)}{\sigma(\bar{\nu} p \to \mu^+ n \pi^o)} \tag{2.27}$$

The ratio $\tilde{R}^{\bar{\nu}}_{0}$ has been corrected for the fact that the Gargamelle mixture is not an isoscalar target. The factor of 1.22 is just the proton-to-neutron ratio for this target.

Figures 6 and 7 show the differential cross-sections for the processes $\nu p \to \nu p \pi^o$ and $\bar{\nu} p \to \bar{\nu} p \pi^o$ respectively, plotted against the pion-nucleon mass $M_{p\pi^o}$. Curves are presented for regions A, B, C, and D. The experimental results[6] for these mass plots are quite rough because of limited statistics (only a selected sample of events are shown) and because of nuclear distortions, but they clearly show a strong excitation of the $\Delta(1232)$ resonance. As one might expect, the isovector regions A and B show strong resonance production and are in general agreement with the shapes of the experimental plots. Regions C and D, being largely

isoscalar, display very weak resonance production in sharp disagreement with the data. The theoretical curves plotted are arbitarily normalized to the experimental data but they are absolutely normalized to each other. Thus, we see that cross-sections for regions C and D are many times smaller than those for A and B, and that region B has a noticeably smaller cross-section for antineutrinos than region A.

Detailed comparison with the cross-section ratios from Gargamelle[6] supports the general picture given in the mass plots of Figs. 6 and 7. Our results are shown in Figs. 2–4 where the area allowed by both elastic and pion-exclusive data is the cross-hatched region. Regions which give an isoscalar neutral current are strongly eliminated by this analysis. For example, regions C and D give cross-section ratios which are approximately an order of magnitude lower than the data. In addition, the small edge of region B in Fig. 2 which had been allowed by the elastic data is now eliminated because it gives too small a cross-section ratio for the antineutrino data. Although our allowed region does come fairly close to region B, those points close to B require the entire 1.6 standard deviation experimental error and 30% theoretical error to be considered as allowed. Any tightening of these conditions at all would eliminate these areas.

Only one region remains allowed by all four types of neutrino scattering results. This is the area (part of region A) shaded by dots in Figs. 2 and 3. This gives a unique determination of the u and d quark coupling-constants for neutral-current interactions. Our final results are also plotted in Fig. 1. The area allowed by both elastic and pion-exclusive data is shaded with lines while that allowed by all

data is shaded with both dots and lines. Note that correlations between left and right couplings are not shown in Fig. 1. Thus, a small corner of the upper dotted region in the right-coupling plane which appears to be allowed by elastic and pion-exclusive data does not in fact represent a region allowed by all experiments as is clearly shown in Fig. 2.

Our final determination for the u and d quark couplings is:[27]

$$u_L = 0.35 \pm 0.07 \qquad u_R = -0.19 \pm 0.06$$

$$d_L = -0.40 \pm 0.07 \qquad d_R = 0.0 \pm 0.11$$

where errors shown are 90% confidence limits and an overall sign convention ($u_L \geq 0$) has been assumed.

E. Comparison with Gauge Theories

Until now we have made no reference to the various gauge theories of the weak and electromagnetic interactions. A comparison of our results with a variety of models is shown in Fig. 8. The two lines with tick-marks show the quark couplings of the Weinberg-Salam model[2] for tenth values of $\sin^2\theta_W$. While the low-energy pion-inclusive data[4] shown in Fig. 8b (for the right-coupling plane) appear to favor values of $\sin^2\theta_W$ from 0.25 to 0.32, the high-energy data[7] allows the range 0.2 to 0.32 which is entirely consistent with the values allowed in the left-coupling plane (Fig. 8a). Thus, the Weinberg-Salam model with $\sin^2\theta_W$ between 0.2 and 0.3 is in excellent agreement with our results. The consistency between $\sin^2\theta_W$ values determined from the left and right-coupling planes indicates that the Z^o to $W^{\pm}$ mass ratio,

$$\frac{M_{Z^o}}{M_{W^\pm}} = \frac{1}{\cos\theta_W} \tag{2.28}$$

predicted by the Weinberg-Salam model with the minimal Higgs boson structure (one or more doublets) is correct. If this mass ratio were not as predicted, the model would be ruled out (for example, one might find that $\sin^2\theta_W \approx 0.1$ was required by the left-coupling plane, but that $\sin^2\theta_W \approx 0.4$ was required in the right-coupling plane). These successes of the Weinberg-Salam model are quite remarkable.

Most other gauge models are not consistent with these results. The points marked A, B, and C (not to be confused with regions A, B, and C discussed above) in Fig. 8b show the results of other SU(2)×U(1) models. All of these have left-handed couplings identical to those of the Weinberg-Salam model (i.e. they have the coupling $(ud)_L$). Choosing $\sin^2\theta_W = 0.3$ so that all of these models are in agreement with our allowed region in the left-coupling plane, we find that the corresponding points in the right-coupling plane lie far from our allowed right-coupling region. Model A has a right-handed doublet[28] $(ub)_R$, model B a right-handed doublet[29] $(td)_R$, and C, also known as the vector model,[30] has both of these. All of these models are eliminated by our analysis and cannot be saved by varying the Z^o to $W^\pm$ mass ratio. Other SU(2)×U(1) models[31] involving -4/3 and 5/3 charged quarks are also ruled out.

It is important to realize that the absence of right-handed charged-currents in these SU(2)×U(1) models is determined algebraically from our neutral-current results. If one writes

$$J_\mu^{CC} = \bar{q}C\gamma_\mu(1+\gamma_5)q \tag{2.29}$$

$$J_\mu^{NC} = \bar{q}C^o\gamma_\mu(1+\gamma_5)q - 2\sin^2\theta_W J_\mu^{em} \qquad (2.30)$$

where q is the vector (u,c,d,s,...) and C is a matrix giving the appropriate charged current of a given SU(2)×U(1) model; then C^o describing the neutral current is

$$C^o = [C, C^\dagger] \qquad (2.31)$$

Thus, for example, right-handed coupling of u and d quarks to b and t quarks of arbitrarily high mass can be ruled out.

The application of our results is, of course, not limited to SU(2)×U(1) models. For example, there are two SU(3)×U(1) models ruled out by the data. One, labeled D in Fig. 8, has the u quarks in a right-handed singlet[32] and the other, labeled E, has the u quark in a right-handed triplet.[33] (For E, we have chosen the parameters of the model so as to place u_L and d_L in the allowed region of Fig. 8a).

These results also apply to models with more than one Z^o boson. For example, the $SU(2)_L \times SU(2)_R \times U(1)$ model[34] can be chosen to give the same values of u_L, d_L, u_R and d_R as the Weinberg-Salam model and so it is allowed by our analysis. In fact, it has been shown[35] that, at zero-momentum transfer, the neutral-current interactions of neutrinos in an SU(2)×G×U(1) gauge theory are the same as in the corresponding SU(2)×U(1) theory if neutrinos are neutral under G. Thus, all such models "corresponding" to the Weinberg-Salam model are allowed by our analysis.

Comparison of Fig. 8 with Fig. 1 shows that even if one ignores the results of pion-inclusive experiments and uses the entire region allowed by elastic and pion-exclusive results our conclusions about these

models are unchanged. Only the Weinberg-Salam model and models equivalent to it for neutrino scattering experiments are allowed by our analysis.

Since the Weinberg-Salam model is in such good agreement with our results, we now consider it in more detail. The predictions of the model as a function of $\sin^2\theta_W$ are compared with the data for all four types of neutrino scattering experiments in Figs. 9–15. All data points are shown with 90% confidence limit error bars, except in Fig. 9 where one standard deviation is shown. The deep-inelastic results[3] from CDHS and from four other groups are shown in Fig. 9. There is general agreement in the data from all groups. π^+ to π^- multiplicity ratios from neutrino and antineutrino-induced inclusive pion production[4] are displayed in Fig. 10. One can see from this figure why the Weinberg-Salam model lies on the edge of the allowed region of Fig. 8b. Figure 11 gives the new HPW elastic scattering data[5] (with only statistical errors shown). The Q^2 dependence of the elastic cross-sections is consistent with that expected by the Weinberg-Salam model. Figures 12–15 show results for the exclusive-pion production cross-sections ratios[6] defined in Eqs. (2.22)–(2.27). In addition, theoretical curves are given for the following ratios not measured by the Gargamelle antineutrino group:

$$R_0^{\bar{\nu}} = \frac{\sigma(\bar{\nu}p \to \bar{\nu}p\pi^o) + \sigma(\bar{\nu}n \to \bar{\nu}n\pi^o)}{2\,\sigma(\bar{\nu}p \to \mu^+ n\pi^o)} \tag{2.32}$$

$$R_{n\pi^+}^{\bar{\nu}} = \frac{\sigma(\bar{\nu}p \to \bar{\nu}n\pi^+)}{\sigma(\bar{\nu}p \to \mu^+ n\pi^o)} \tag{2.33}$$

An error bar is shown for the curves of the Weinberg-Salam model reflecting the 30% theoretical uncertainty we assigned to the pion-production model. One can see in Fig. 12 that $R^{\nu}_{p\pi^o}$ and $R^{\nu}_{n\pi^o}$ are predicted to be approximately equal for the model whereas their measured values[6] are quite different; nonetheless both are consistent with the data within the limits. Actually, the equality of these two ratios was found to be quite model independent.

In summary, the neutral-current couplings of u and d quarks are known and are successfully predicted by the Weinberg-Salam model. Comparison of this model for $\sin^2\theta_W = 0.25$ with our results is presented in Table 1.

TABLE 1

	Results of this analysis	W-S ($\sin^2\theta_W$=0.25)
u_L	0.35 ± 0.07	0.33
d_L	-0.40 ± 0.07	-0.42
u_R	-0.19 ± 0.06	-0.17
d_R	0.0 ± 0.11	0.08

III. ELECTRON COUPLINGS

The weak neutral-current couplings of the electron are measured in neutrino-electron scattering ($\nu e \to \nu e$), and in parity-violation experiments. If we assume that the neutral-current is coupled to a single Z^o boson, the determination of the u and d quark couplings from Section II allows us to analyze the results of parity-violation experiments in a model-independent manner.[36] New experimental results[10] from SLAC then

provide a substantial improvement in the determination of the neutral-current couplings of the electron.

Let us define e_L and e_R as the coefficients in the effective neutrino-electron neutral-current interaction:

$$\mathscr{L} = (G/\sqrt{2})\bar{\nu}\gamma^{\mu}(1+\gamma_5)\nu \left[e_L\bar{e}\gamma_{\mu}(1+\gamma_5)e + e_R\bar{e}\gamma_{\mu}(1-\gamma_5)e\right] \tag{3.1}$$

and define g_V and g_A as

$$g_V = e_L + e_R \tag{3.2}$$

$$g_A = e_L - e_R \tag{3.3}$$

The cross-section for muon-neutrino electron ($\nu_\mu e$) and muon-antineutrino electron ($\bar{\nu}_\mu e$) scattering is

$$\frac{d\sigma^{\nu,\bar{\nu}}}{dE_e} = \frac{G2M_e}{2\pi}\left[(g_V \pm g_A)^2 + (g_V \mp g_A)^2\left(1 - \frac{E_e}{E_\nu}\right)^2 + \left(g_A^2 - g_V^2\right)\frac{M_e E_e}{E_\nu^2}\right] \tag{3.4}$$

where the bottom signs are for antineutrinos. For electron-antineutrino electron ($\bar{\nu}_e e$) scattering there is an additional annihilation term (through the charged current), so that in Eq. (3.4) one makes the replacements $g_V \to g_V + 1$ and $g_A \to g_A + 1$.

Knowledge of these various neutrino-electron cross-sections leads to allowed regions in a g_V-g_A plot which are elliptical annuli. These are shown in Fig. 16. In this figure we have plotted the highest upper limits and the lowest lower limits coming from the Gargamelle-PS and Aachen-Padua results.[8] High-energy Gargamelle-SPS data[8] on $\nu_\mu e$ scattering are in conflict with these low-energy results and are also in conflict with new high-energy Fermilab data.[8] The Fermilab result for $\nu_\mu e$ scattering is in complete agreement with that presented in Fig. 16 from the low-energy data.

So far we have not required the assumption of a single Z^o boson. However, to make use of the results of the parity-violation experiments this assumption is needed. Results have been reported for parity-violation in atomic transitions in bismuth.[9] The optical rotation, ρ, which is measured is proportional to the $V_{had}\ A_{elec}$ interference term; the $A_{had}\ V_{elec}$ term is relatively suppressed. According to theoretical calculations, the optical rotations for the two transitions which have been measured are given by:

$$\rho \approx -4.4 \times 10^{-9}\ V_{had}\ g_A \qquad \text{radians (for } 8757\text{Å}) \qquad (3.5)$$

$$\rho \approx -6.0 \times 10^{-9}\ V_{had}\ g_A \qquad \text{radians (for } 6476\text{Å}) \qquad (3.6)$$

where

$$V_{had} = (2u_L+d_L+2u_R+d_R)Z + (u_L+2d_L+u_R+2d_R)N \qquad (3.7)$$

(Z=83 and N=126 for bismuth) .

Two experimental groups report results consistent with zero: the Washington group[9] measures $\rho=(-0.5 \pm 1.7) \times 10^{-8}$ for the 8757Å transition and the Oxford group[9] $\rho=(2.7 \pm 4.7) \times 10^{-8}$ for the 6476Å transition. By contrast, the Novosibirsk experiment[9] found $\rho=(-21 \pm 6)\times 10^{-8}$ for the 6476Å transition. Assuming that there exists only one Z^o boson, then the quark couplings of Section II imply that $g_A \approx 0.0 \pm 0.06$ for the first two experiments and $g_A \approx -0.4 \pm 0.17$ for the Novosibirsk experiment. These results are plotted as dotted bands in Fig. 16 where 90% confidence limits have been used and the effects of error bars for the quark couplings have been included.

In order to resolve this conflict, we make use of a very recent SLAC experiment[10] involving the deep-inelastic scattering of polarized electrons off deuterium and hydrogen targets. In this experiment one measures the asymmetry between the cross-sections σ_p and σ_a for electrons polarized parallel and antiparallel to the beam. Weak parity-violating effects will produce a non-zero asymmetry value. The asymmetry is sensitive to both $V_{had}\,A_{elec}$ and $A_{had}\,V_{elec}$ terms, and furthermore involves no difficult atomic or nuclear calculations.

For an isoscalar target (deuterium) the asymmetry (see Cahn and Gilman, Ref. 37) is (with the one Z^o assumption):

$$\frac{d\sigma_p - d\sigma_a}{d\sigma_p + d\sigma_a} = 64\times10^{-5}\ Q^2 \left\{\left[\frac{2}{3}\ (u_L+u_R) - \frac{1}{3}\ (d_L+d_R)\right] g_A + \left[\frac{1-(1-y)^2}{1+(1-y)^2}\right] \times \left[\frac{2}{3}\ (u_L-u_R) - \frac{1}{3}\ (d_L-d_R)\right] g_V\right\} \tag{3.8}$$

where Q^2 is in GeV^2 and y is the fractional energy loss of the electron.

The SLAC results[10] are for Q^2=1.4 GeV^2 and y=0.21. The asymmetry divided by Q^2 was measured to be -9.6 ± 1.7 (results are preliminary and 0.9 of the uncertainty is systematic). The allowed region in the g_V-g_A plane coming from this value and using a single Z^o hypothesis is the striped band in Fig. 17. The width of this band reflects 90% confidence level errors for both the asymmetry and for our quark-coupling values. Also shown in this figure is the overlap region from νe scattering experiments obtained from Fig. 16 and the two bands (shaded with dots) coming from the atomic parity-violation experiments.

The predictions of the Weinberg-Salam model for this asymmetry for various values of $\sin^2\theta_W$ are shown in Fig. 18. Also shown are the results if the electron is given a right-handed coupling $(N_e e^-)_R$ in addition to its usual left-handed coupling $(\nu_e e^-)_L$, but assuming no other changes to the Weinberg-Salam model are made. Although the present SLAC data favor the conventional version over this "hybrid" model, future asymmetry measurements at other y-values should clearly distinguish between these two cases.

The recent SLAC results taken in conjunction with the νe scattering data appear to be in conflict with the Washington-Oxford results for bismuth as can be seen in Fig. 17. Excluding the Washington-Oxford data, it is clear that the Weinberg-Salam model with $\sin^2\theta_W$ between 0.2 and 0.3 is in complete agreement with these electron experiments. This is the same range of $\sin^2\theta_W$ as we found in Sec. II for quark couplings.

IV. CONCLUSIONS

We have provided a unique determination of the weak neutral-current couplings of u and d quarks. In addition, with the assumption of a single Z^o boson we have presented an almost unique determination of the electron couplings. These results give substantial support to the Weinberg-Salam model as the correct unified theory of weak and electromagnetic interactions.

In the future, improvements can be made in several areas. There is a need for more high-energy pion-inclusive data; these data played an important role in our analysis, and it would be helpful to avoid dependence on low-energy results. Similar information could be obtained from deep-inelastic scattering off protons and off neutrons

(as opposed to isoscalar targets), and from deuteron dissociation experiments. Further study of exclusive-pion production would also be helpful.

For electron coupling determination, a crucial additional step is the measurement of the polarized-electron asymmetry at different values of y. Also, the conflicts in atomic-parity violation experiments should be resolved, and experiments on hydrogen and deuterium should be performed to verify the SLAC results. At the PEP and PETRA storage rings, measurement of the muon asymmetry in $e^+e^- \to \mu^+\mu^-$ will provide information not only about the electron couplings but also about the muon couplings.

ACKNOWLEDGMENTS

For useful discussion we would like to thank S. Adler, J. Bjorken, G. Feldman, F. Gilman, P. Lepage, J. Marriner, J. Martin, C. Matteuzzi, E. Monsay, F. Nezrick, Y.-J. Ng, E. Paschos, C. Prescott, F. Reines, B. Roe, C. Sinclair, H. Sobel, L. Sulak, and S. Weinberg. This work was supported in part by the Department of Energy.

Appendix A

There are two types of modifications to Eqs. (2.6)-(2.7) for deep-inelastic scattering which are important. The first accounts for the contributions of "sea" quarks (quark-antiquark pairs in the nucleon) to the scattering cross-sections. The second accounts for an experimental cut $E_{hadron} > E_0$ which neutral-current experiments always have (although the data are sometimes extrapolated to $E_{hadron}=0$).

The effect of the E_{hadron} cut is to modify the helicity factors of 1/3 and 1 which result from integration of the terms $(1-y)^2$ and 1 in the differential cross-sections. Only the ratio of these terms enters our calculations so that we define ξ (for $E_{hadron} > E_0$) as:

$$\xi \equiv \frac{\int dE_\nu \; E_\nu \; \rho_\nu \int_{E_0/E_\nu}^{1} dy \; (1-y)^2}{\int dE_\nu \; E_\nu \; \rho_\nu \int_{E_0/E_\nu}^{1} dy} \tag{A1}$$

where ρ_ν is the spectrum of incoming neutrinos. For $E_0=0$ one has $\xi = 1/3$.

The ratio α of nucleon momentum carried by antiquarks to that by quarks ($\alpha \equiv \bar{q}/q$) is a function of Q^2 in QCD. Let us, however, make the approximation of choosing α at the average Q^2 of the given experiment. Then (neglecting s and c quarks) the neutral to charged-current ratios (Eqs. (2.6)-(2.7) for deep-inelastic scattering are now:

$$R_\nu = \left[(1+\alpha\xi)(u_L^2+d_L^2) + (\xi+\alpha)(u_R^2+d_R^2)\right]/1 \tag{A2}$$

$$R_{\bar{\nu}} = \left[(\xi+\alpha)(u_L^2+d_L^2) + (1+\alpha\xi)(u_R^2+d_R^2)\right]/\xi \tag{A3}$$

These can be solved so that

$$u_L^2+d_L^2 = \frac{(1+\alpha\xi)R_\nu-(\xi+\alpha)\xi\ R_{\bar{\nu}}}{(1+\alpha\xi)^2 - (\xi+\alpha)^2} \tag{A4}$$

$$u_R^2+d_R^2 = \frac{(\xi+\alpha)R_\nu-(1+\alpha\xi)\xi\ R_{\bar{\nu}}}{(\xi+\alpha)^2 - (1+\alpha\xi)^2} \tag{A5}$$

Appendix B

One can apply the corrections of Appendix A to pion-inclusive scattering. Using ξ as defined in Eq. (A1) and $\alpha \equiv \bar{q}/q$, Eqs. (2.12a and b)can be modified to read (with the same approximations as in Appendix A):

$$\left(\frac{N_{\pi^+}}{N_{\pi^-}}\right)_{\nu} = \frac{\left[u_L^2+\xi u_R^2+\alpha(\xi d_L^2+d_R^2)\right]\eta + \left[d_L^2+\xi d_R^2+\alpha(\xi u_L^2+u_R^2)\right]}{\left[u_L^2+\xi u_R^2+\alpha(\xi d_L^2+d_R^2)\right] + \left[d_L^2+\xi d_R^2+\alpha(\xi u_L^2+u_R^2)\right]\eta} \equiv R_{\nu}^{\pi} \tag{B1}$$

$$\left(\frac{N_{\pi^+}}{N_{\pi^-}}\right)_{\bar{\nu}} = \frac{\left[u_R^2+\xi u_L^2+\alpha(\xi d_R^2+d_L^2)\right]\eta + \left[d_R^2+\xi d_L^2+\alpha(\xi u_R^2+u_L^2)\right]}{\left[u_R^2+\xi u_L^2+\alpha(\xi d_R^2+d_L^2)\right] + \left[d_R^2+\xi d_L^2+\alpha(\xi u_R^2+u_L^2)\right]\eta} \equiv R_{\bar{\nu}}^{\pi} \tag{B2}$$

These can be solved to give

$$\frac{R_{\nu}^{\pi}-\eta}{1-\eta R_{\nu}^{\pi}} = \frac{d_L^2+\xi d_R^2 + \alpha(\xi u_L^2+u_R^2)}{u_L^2+\xi u_R^2 + \alpha(\xi d_L^2+d_R^2)} \tag{B3}$$

$$\frac{R_{\bar{\nu}}^{\pi}-\eta}{1-\eta R_{\bar{\nu}}^{\pi}} = \frac{d_R^2+\xi d_L^2 + \alpha(\xi u_R^2+u_L^2)}{u_R^2+\xi u_L^2 + \alpha(\xi d_R^2+d_L^2)} \tag{B4}$$

The quantities on the left-side of Eqs. (B3) and (B4) are determined experimentally.

Appendix C

The cross-section[18] for elastic neutral-current (and charged current) νN scattering is

$$\frac{d\sigma}{dQ^2} = \frac{G^2 m^2}{8\pi E_\nu^2}\left[A \pm B\,\frac{(s-u)}{m^2} + C\,\frac{(s-u)^2}{m^4}\right]\varepsilon \tag{C1}$$

where (+) refers to neutrinos and (-) to antineutrinos, and $(s-u)=(4mE_\nu - Q^2)$. For νn scattering (as opposed to νp scattering), the isovector terms in Eqs. (2.16) and (2.17) should be multiplied by -1. Setting $m_\mu^2=0$ one has

$$A = \frac{Q^2}{m^2}\left[F_A^2\left(1+\frac{Q^2}{4m^2}\right) - \left(F_1^2 - \frac{Q^2}{4m^2}F_2^2\right)\left(1-\frac{Q^2}{4m^2}\right) + \frac{Q^2}{m^2}F_1F_2\right] \tag{C2}$$

$$B = \frac{Q^2}{m^2}F_A(F_1+F_2) \tag{C3}$$

$$C = \frac{1}{4}\left(F_A^2+F_1^2 + \frac{Q^2}{4m^2}F_2^2\right) \tag{C4}$$

where ε is a Clebsch-Gordon factor given by

$$\varepsilon = \begin{cases} \tfrac{1}{4} \text{ for neutral currents} \\ 1 \text{ for charged currents} \end{cases} \tag{C5}$$

Appendix D

The calculation of exclusive-pion production using the model of Adler[22-24] begins with the vector and axial-vector Born amplitudes for isovector $\left(I = \frac{1}{2} \text{ and } \frac{3}{2}\right)$ and isoscalar terms. These are given in Ref. 22 except for the isoscalar axial-vector terms[24]

$$A_1^{(o)} = g_r \frac{g_A^S(k^2)}{2m} \left(\frac{1}{\nu_B - \nu} - \frac{1}{\nu_B + \nu}\right) \tag{D1}$$

$$A_3^{(o)} = g_r \frac{g_A^S(k^2)}{2m} \left(\frac{1}{\nu_B - \nu} + \frac{1}{\nu_B + \nu}\right) \tag{D2}$$

where the notation is the same as in Ref. 22 and $g_A^S(k^2)$ is equal to the second term in Eq. (2.17).

The amplitudes must be modified to account for current algebra corrections (Ref. 23). These come from using the current algebra relation:

$$T\{\partial^\mu J_\mu^5 \mathcal{J}\} = -\delta(x_0)[J_0^5, \mathcal{J}] + \partial^\mu T\{J_\mu^5 \mathcal{J}\} \tag{D3}$$

(where T indicates time-ordered product, and $\mathcal{J}$ is the weak current of interest). Taking Fourier transforms and then the matrix element between nucleon states for each piece of Eq. (D3), one finds from PCAC that the left side is proportional to the desired matrix element $\langle N\pi | \mathcal{J}(0) | N \rangle$. The first term of the right side leads to additional form-factor terms. The second term containing the J^5 current with axial-vector couplings rather than the pseudo-scalar couplings assumed for the pion, implies certain vertex corrections. The resulting five correction terms are given in Ref. 23. $0(q)$ corrections ($q \equiv$ pion momentum) are also discussed in that paper.[38]

Next, the multipoles for given orbital angular momentum of the pion-nucleon system are calculated by integrating the appropriate amplitudes over $\cos\phi$. ϕ is the angle between the pion momentum and the difference in momenta of the incoming and outgoing neutrinos in the isobaric frame (pion-nucleon rest frame). Those multipoles for isospin $\frac{3}{2}$ and pion-nucleon spin $\frac{3}{2}$ are now modified by a phase $e^{i\delta_R}$ and an enhancement factor. We used the parameterization

$$e^{i\delta_R} = \frac{\left(q_0 - q_0^R\right) - i\,\frac{\Gamma}{2}}{\left[\left(q_0 - q_0^R\right)^2 + \frac{\Gamma^2}{4}\right]^{\frac{1}{2}}} \tag{D4}$$

where $q_0^R = 0.268$ GeV,

$$\Gamma = \frac{9.04\ |\vec{q}|^3}{\left(q_0 + q_0^R\right)\left(1 + 25.9\ |\vec{q}|^2\right)}\ (\text{GeV}) \tag{D5}$$

and q_0 and $\vec{q}$ are the energy and momentum of the pion in the isobaric frame.

The cross-section is obtained by summing over all appropriate multipoles with orbital angular momentum of 0 and 1 (assuming higher terms are negligible). Finally, one integrates over k^2 ($k \equiv$ momentum transfer) and W ($W \equiv M_{N\pi}$ has an upper limit of the smaller of 1.4 GeV and the kinematic limit).

The importance of keeping the non-resonant $I = \frac{1}{2}$ terms is indicated by the neutral-current data:[6]

$$\frac{\sigma(\nu p\pi^0) + \sigma(\nu n\pi^0)}{\sigma(\nu n\pi^+) + \sigma(\nu p\pi^-)} = 1.14 \pm 0.3 \tag{D6}$$

where 2.0 is predicted if $I = \frac{1}{2}$ terms are ignored, and

$$\frac{\sigma(\bar{\nu}p\pi^{o}) + \sigma(\bar{\nu}n\pi^{o})}{\sigma(\bar{\nu}p\pi^{-})} = 2.4 \begin{matrix} + 0.8 \\ - 0.6 \end{matrix} \qquad \text{(D7)}$$

where 4.44 is predicted if $I = \frac{1}{2}$ terms are ignored. A purely $I = \frac{3}{2}$ theory has a 0.02 confidence level.[6]

It is interesting to note that the current algebra corrections result in an induced axial-vector contribution even in the absence of any axial-vector terms in the weak current at the Born level. The manner in which the current algebra corrections enter is such that in the absence of final-state interactions, the induced axial-vector pieces would cancel out in the cross-sections (the Clebsch-Gordon coefficients conspire to cause this cancellation). However, because the $I = \frac{3}{2}$ and not the $I = \frac{1}{2}$ terms are enhanced, this cancellation does not occur, and the induced axial-vector contribution survives.

REFERENCES

1. L. F. Abbott and R. M. Barnett, Phys. Rev. Lett. 40, 1303 (1978); R. M. Barnett, report no. SLAC-PUB-2131 (1978), to appear in the proceedings of the Neutrinos-78 Conference, Purdue University, April 1978.

2. S. Weinberg, Phys. Rev. Lett. 19, 1264 (1967); A. Salam, in Elementary Particle Physics: Relativistic Groups and Analyticity, edited by N. Svartholm (Almquist and Wiksell, Stockholm, 1968), p. 367.

3. M. Holder et al. (CDHS), Phys. Lett. 72B, 254 (1977); J. Blietschau et al. (Gargamelle), Nucl. Phys. B118, 218 (1977); A. Benvenuti et al. (HPWF), Phys. Rev. Lett. 37, 1039 (1976); P. Wanderer et al. (HPWF), Phys. Rev. D17, 1679 (1978); F. S. Merritt et al. (CF), Phys. Rev. D17, 2199 (1978); K. Schultze (BEBC), in Proc. 1977 Int. Symp. on Lepton and Photon Interactions at High Energies, edited by F. Gutbrod (DESY, Hamburg, 1977) p. 359, and P. C. Bosetti et al., report no. Oxford-NP-20/78 (1978).

4. H. Kluttig, J. G. Morfin and W. Van Doninck, Phys. Lett. 71B, 446 (1977).

5. L. Sulak, Harvard report, to appear in the Proceedings of the Neutrinos-78 Conference, Purdue University, April 28-May 2, 1978; J. B. Strait and W. Kozanecki, Harvard University Ph.D. Theses (1978); D. Cline et al., Phys. Rev. Lett. 37, 252 and 648 (1976); see also W. Lee et al., Phys. Rev. Lett. 37, 186 (1976); M. Pohl et al., Phys. Lett. 72B, 489 (1978).

6. W. Krenz et al., report no. CERN/EP/PHYS 77-50 (1977); O. Erriques et al., Phys. Lett. 73B, 350 (1978); see also S. J. Barish et al., Phys. Rev. Lett. 33, 448 (1974); W. Lee et al., Phys. Rev. Lett. 38, 202 (1977).

7. J. Marriner, report no. LBL-6438 (1977), Univ. of California Ph.D. Thesis.

8. P. Alibran et al. (Gargamelle-PS: $\nu_\mu e$), Phys. Lett. 74B, 422 (1978); J. Blietschau et al. (Gargamelle-PS: $\bar{\nu}_\mu e$), Nucl. Phys. B114, 189 (1976); F. Reines et al. ($\bar{\nu}_e e$), Phys. Rev. Lett. 37, 315 (1976); M. Baldo-Ceolin (Aachen-Padua: $\nu_\mu e$ and $\bar{\nu}_\mu e$), to appear in the proceedings of the Neutrinos-78 Conference, Purdue University, April 28-May 2, 1978; P. Alibran et al. (Gargamelle-SPS: $\nu_\mu e$), report no. CERN/EP/PHYS 78-6 (1978); C. Baltay et al. (Brookhaven-Columbia: $\nu_\mu e$), Fermilab report (1978).

9. P. E. G. Baird et al. (Oxford and Washington), Nature 264, 528 (1976); P. G. H. Sandars (Oxford), in Proc. 1977 Int. Symp. on Lepton and Photon Interactions at High Energies, edited by F. Gutbrod (DESY, Hamburg, 1977) p. 599; N. Fortson (Washington), to appear in the proceedings of the Neutrinos-78 Conference, Purdue University, April 28-May 2, 1978; L. M. Barkov and M. S. Zolotorev (Novosibirsk), Pisma Zh.Eksp.Teor.Fiz.(JETP Lett.) 26, 379 (1978).

10. C. Prescott, in a SLAC colloquium (June 1978) and private communication.

11. S. L. Glashow, J. Iliopoulos and L. Maiani, Phys. Rev. D2, 1285 (1970).

12. Reviews of the parton model: J. Ellis, in Weak and Electromagnetic Interactions at High Energy, edited by R. Balian and C. H. Llewellyn Smith (North-Holland, Amsterdam, 1977) p. 5; T.-M. Yan, Ann. Rev. Nucl. Sci. 26, 199 (1976); see also J. D. Bjorken, in Proc. of Summer Institute on Particle Physics, August 2-13, 1976, edited by M. C. Zipf (SLAC, Stanford, 1976), p. 1.

13. This number was given by the CDHS group (Ref. 3 and H. Wahl, to appear in the proceedings of the Neutrinos-78 Conference, Purdue University, April 28-May 2, 1978).

14. L. M. Sehgal, Phys. Lett. 71B, 99 (1977); P. Q. Hung, Phys. Lett. 69B, 216 (1977); P. Scharbach, Nucl. Phys. B82, 155 (1974); and Ref. 1.

15. J. Dakin and G. Feldman, Phys. Rev. D8, 2862 (1975); M. Haguenauer, in Proc. XVIII Int. Conf. on High Energy Physics, London, 1-10 July 1974, (Science Research Council, Rutherford Laboratory, 1974), p. IV-37; these data were analyzed by L. M. Sehgal, Nucl. Phys. B90, 471 (1975); P. Q. Hung, Phys. Lett. 69B, 216 (1977); J. Okada and S. Pakvasa, Nucl. Phys. B112, 400 (1976).

16. P. Q. Hung and J. J. Sakurai, Phys. Lett. 72B, 208 (1977); P. Langacker and D. P. Sidhu, Phys. Lett. 74B, 233 (1978); G. Ecker, Phys. Lett. 72B, 450 (1978); D. P. Sidhu and P. Langacker, Report No.BNL-24393 (1978).

17. J. F. Martin et al., report no. SLAC-PUB-2038 (1977); J. F. Martin, private communication.

18. S. Weinberg, Phys. Rev. D5, 1412 (1972); R. M. Barnett, Phys. Rev. D14, 2990 (1976); C. H. Albright et al., Phys. Rev. D14, 1780 (1976); V. Barger and D. V. Nanopoulos, Nucl. Phys. B124, 426 (1977); D. P. Sidhu, Phys. Rev. D14, 2235 (1976); F. Martin, Nucl. Phys. B104, 111 (1976); J. D. Bjorken, Ref. 12.

19. P. Q. Hung, Phys. Rev. D17, 1893 (1978); R. M. Barnett, Ref. 18.

20. G. Ecker, Phys. Lett. 72B, 450 (1978).

21. E. H. Monsay, Argonne report ANL-HEP-PR-78-08 (1978).

22. S. L. Adler, Ann. Phys. 50, 189 (1968).

23. S. L. Adler, Phys. Rev. D12, 2644 (1975).

24. S. L. Adler, et al., Phys. Rev. D13, 1216 (1976).

25. This point is discussed further in Appendix D.

26. These requirements for exclusive-pion production are very similar to those in Ref. 1 where allowed regions were those within a factor of two of the data.

27. These numbers are very slightly different from those in Ref. 1 because of 1) modified requirements for exclusive-pion production (see footnote 26), 2) inclusion of sea effects in inclusive-pion production, 3) new elastic data.

28. R. M. Barnett, Phys. Rev. Lett. 34, 41 (1975), Phys. Rev. D11, 3246 (1975); P. Fayet, Nucl. Phys. B78, 14 (1974); F. Gürsey and P. Sikivie, Phys. Rev. Lett. 36, 775 (1976); P. Ramond, Nucl. Phys. B110, 214 (1976).

29. R. M. Barnett, Phys. Rev. D13, 671 (1976).

30. A. De Rújula et al., Phys. Rev. D12, 3589 (1975); F. A. Wilczek et al., Phys. Rev. D12, 2768 (1975); H. Fritzsch et al., Phys. Lett. 59B, 256 (1975); S. Pakvasa et al., Phys. Rev. Lett. 35, 702 (1975).

31. See R. M. Barnett, Phys. Rev. D15, 675 (1977).

32. B. W. Lee and S. Weinberg, Phys. Rev. Lett. 38, 1237 (1977); B. W. Lee and R. E. Shrock, Phys. Rev. D17, 2410 (1978); G. Segre and J. Weyers, Phys. Lett. 65B, 243 (1976).

33. R. M. Barnett and L. N. Chang, Phys. Lett. 72B, 233 (1977); R. M. Barnett, L. N. Chang and N. Weiss, Phys. Rev. D17, 2266 (1978); P. Langacker and G. Segre, Phys. Rev. Lett. 39, 259 (1977).

34. J. Pati and A. Salam, Phys. Rev. D10, 275 (1974); H. Fritzsch and P. Minkowski, Nucl. Phys. B103, 61 (1976); R. N. Mohapatra and D. P. Sidhu, Phys. Rev. Lett. 38, 667 (1977); A. De Rújula, H. Georgi and S. L. Glashow, Annals Phys. 109, 242 and 258 (1977).

35. H. Georgi and S. Weinberg, Phys. Rev. D17, 275 (1978); R. Gatto and F. Strocchi, Geneva report (1978).

36. It is conceivable that the neutral-current coupling constant of the neutrino is not equal to one. It is equal to one in all conventional models, and we have assumed this in our interaction Lagrangians (2.1) and (3.1). This would only affect our analysis of parity-violation experiments where it inserts a scale factor. We thank J. J. Sakurai for emphasizing this point.

37. R. N. Cahn and F. J. Gilman, Phys. Rev. D17, 1313 (1978); A. Love, G. G. Ross, and D. V. Nanopoulos, Nucl. Phys. B49, 513 (1972); E. Derman, Phys. Rev. D7, 2755 (1973); N. N. Nikolaev et al., Zh. Eksp. Teor.Fiz.Pis'ma Red. 18, 70 (1973) [JETP Lett. 18, 39 (1973)]; C. H. Llewellyn Smith, in Proceedings of the Seminar on e-p and e-e Storage Rings, edited by J. K. Bienlein, I. Dammann and H. Weidemann (DESY, Hamburg, 1973), p. 95; M. Suzuki, Nucl. Phys. B70, 154 (1974); S. M. Berman and J. R. Primack, Phys. Rev. D9, 2171 (1974); 10, 3895 (E) (1974); W. J. Wilson, ibid. 10, 218 (1974); C. H. Llewellyn Smith in Phenomenology of Particles at High Energies, edited by R. L. Crawford and R. Jennings (Academic, London, 1974), p. 459; C. P. Korthals-Altes et al., Nucl. Phys. B76, 549 (1974); C. H. Llewellyn Smith and D. V. Nanopoulos, ibid. B78, 205 (1974); B83, 544 (E) (1974); M.A.B. Bég and G. Feinberg, Phys. Rev. Lett.

33, 606 (1974); Ya. B. Zeidovich and A. M. Perelomov, Zh.Eksp.Teor. Fiz. 39, 1115 (1960) [Sov. Phys.—JETP 12, 777 (1961)]; S. M. Bilenkii et al., Yad. Fiz. 21, 1271 (1975) [Sov. J. Nucl. Phys. 21, 675 (1976)].

38. Following the suggestion of S. L. Adler (private communication) we have neglected the small $0(q)$ corrections.

TABLE CAPTION

Table 1: The quark-coupling values determined in Sec. II are compared with predictions of the Weinberg-Salam model for $\sin^2\theta_W = 0.25$.

FIGURE CAPTIONS

1. The left (a) and right (b) coupling-constant planes. The lower half of (a) is omitted due to our sign convention $u_L \geq 0$. The annular regions are allowed by deep-inelastic data. The regions shaded with dots are allowed by inclusive-pion results, and the region shaded with lines is allowed by elastic and exclusive-pion data. Unique determination of the quark coupling values is given by the region shaded with both dots and lines.

2. The allowed angles in the coupling planes of Fig. 1 for fixed radii taken at the center of the allowed annulus ($r_L = 0.53$) in the left-coupling plane and at the outer edge of the allowed annulus (r_R=0.22) in the right-coupling plane. The ellipses indicate the regions allowed by inclusive-pion data; going clockwise from the upper-right they are regions A, B, C and D respectively. The area shaded with lines and enclosed with a dotted curve is allowed by elastic data. The region which is cross-hatched is allowed by elastic and exclusive-pion results. The area shaded with dots is the only region allowed by all data.

3. Same as Fig. 2 except that the radius in the right-coupling plane (0.175) has been chosen at the center of the allowed annulus from Fig. 1b.

4. Same as Fig. 2 except that the radius in the right-coupling plane (0.13) has been chosen at the inner edge of the allowed annulus from Fig. 1b. No regions are allowed by the inclusive-pion data for this inner radius.

5. Born diagrams for the exclusive-pion-production analysis. g_r is the pion-nucleon coupling constant.

6. Differential cross-sections for the exclusive-pion-production process $\nu p \rightarrow \nu p\pi^o$ plotted against the mass of the final-state $p\pi^o$ system. Four theoretical curves are compared with the data. The solid curve is for region A, the dashed curve is for B, the dashed and dotted curve is for C and the dotted curve is for D. Data are from Ref. 6.

7. Same as Fig. 6 but for the process $\bar{\nu}p \rightarrow \bar{\nu}p\pi^o$.

8. Various gauge models compared with the allowed coupling-constant region. The lines mark the Weinberg-Salam model for values of $\sin^2\theta_W$ from 0.0 to 0.7. The points labeled A-E are the predictions of various models discussed in the text. For A, B, C, and E, u_L and d_L lie within the allowed region in the left-coupling plane.

9. The ratio of neutral to charged-current deep-inelastic cross-sections for antineutrinos versus that for neutrinos. The curve shows the predictions of the Weinberg-Salam model as a function of $\sin^2\theta_W$ (each tick-mark indicates a tenth value of $\sin^2\theta_W$). The data are from Ref. 3.

10. The ratio of π^+ to π^- multiplicites from inclusive-pion data for antineutrinos versus that for neutrinos. The curve shows the predictions of the Weinberg-Salam model as a function of $\sin^2\theta_W$. The data are from Ref. 4, and 90% confidence limits are shown.

11. The ratio of neutral to charged-current elastic-proton-scattering cross-sections for antineutrinos versus that for neutrinos where $0.4 \leq Q^2 \leq 0.9$ GeV^2. The curve shows the predictions of the Weinberg-Salam model as a function of $\sin^2\theta_W$. The data are from Ref. 5, and only statistical uncertainties are shown (at the 90% confidence level).

12. The bands shaded with dots indicate the exclusive-pion data for the ratios $R^{\nu}_{p\pi^o}$ and $R^{\nu}_{n\pi^o}$ defined in the text. The curves show predictions of the Weinberg-Salam model as a function of $\sin^2\theta_W$. The error bars on these curves indicate a possible 30% uncertainty in the theoretical analysis. Data are from Ref. 6, and 90% confidence limits are shown.

13. Same as Fig. 12 for the ratios $R^{\nu}_{p\pi^-}$ and $R^{\nu}_{n\pi^+}$ defined in the text.

14. Same as Fig. 12 for the ratios $R^{\bar{\nu}}_0$ and $\tilde{R}^{\bar{\nu}}_0$ defined in the text. No data are available for $R^{\bar{\nu}}_0$.

15. Same as Fig. 12 for the ratios $R^{\bar{\nu}}_{p\pi^-}$ and $R^{\bar{\nu}}_{n\pi^+}$ defined in the text. No data are available for $R^{\bar{\nu}}_{n\pi^+}$.

16. Ninety percent confidence limits on g_A and g_V of the electron. Solid curves are for $\bar{\nu}_\mu e$ scattering; dashed curve is for $\nu_\mu e$; dotted curves are for $\bar{\nu}_e e$. For $\bar{\nu}_\mu e$ and $\nu_\mu e$, highest upper limits and lowest lower limits were used from the Aachen-Padua and Gargamelle-PS experiments. The upper (lower) band is for the Washington-Oxford (Novosibirsk) parity-violation experiments assuming a single Z^o boson and the quark-coupling values of Sec. II (including quark-coupling error bars). Data are from Refs. 8 and 9.

17. The overlap regions (90% confidence level) from Fig. 16 are shown. The band shaded with lines is the allowed region from the SLAC polarized-electron-deuteron scattering experiment (Ref. 10) assuming a single Z^o boson and values from Sec. II of quark couplings (including quark error bars). The upper (lower) band shaded with dots is for the Washington-Oxford (Novosibirsk) parity-violation experiments as in Fig. 16. The predictions of the WS model are shown for tenth values of $\sin^2\theta_W$.

18. The predicted asymmetry in the SLAC polarized-electron-deuteron scattering experiment for the WS model (solid curves) and for the "hybrid" model (dashed curves). In this experiment $Q^2 = 1.4$ GeV^2 and $y = 0.21$. σ_p and σ_a refer to cross-sections for electrons polarized parallel and anti-parallel to the beam.

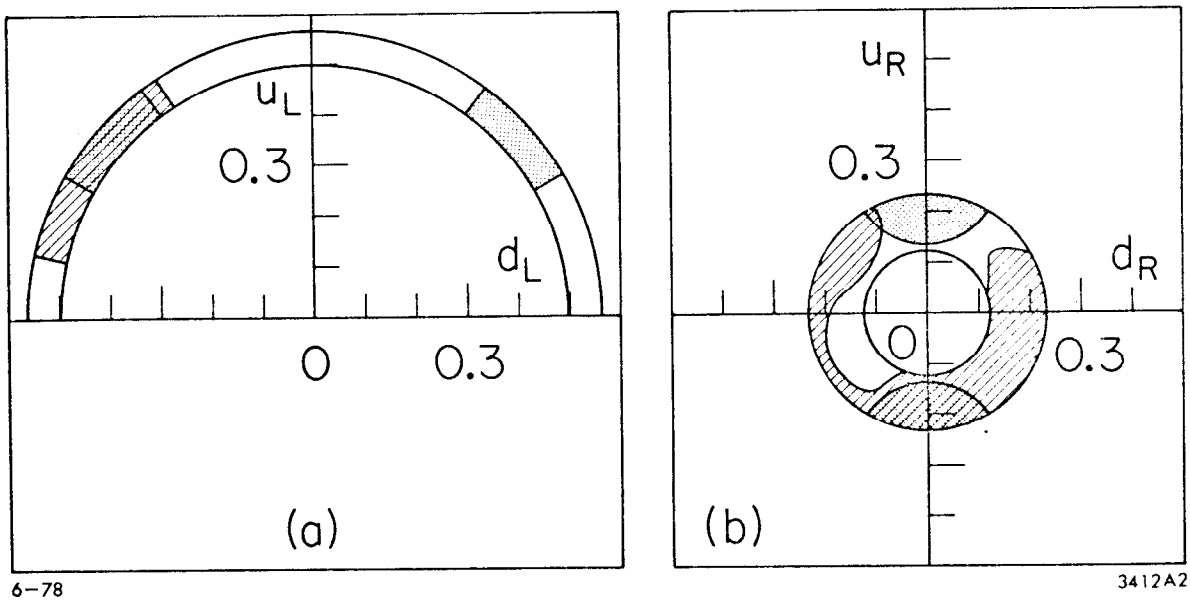

Fig. 1

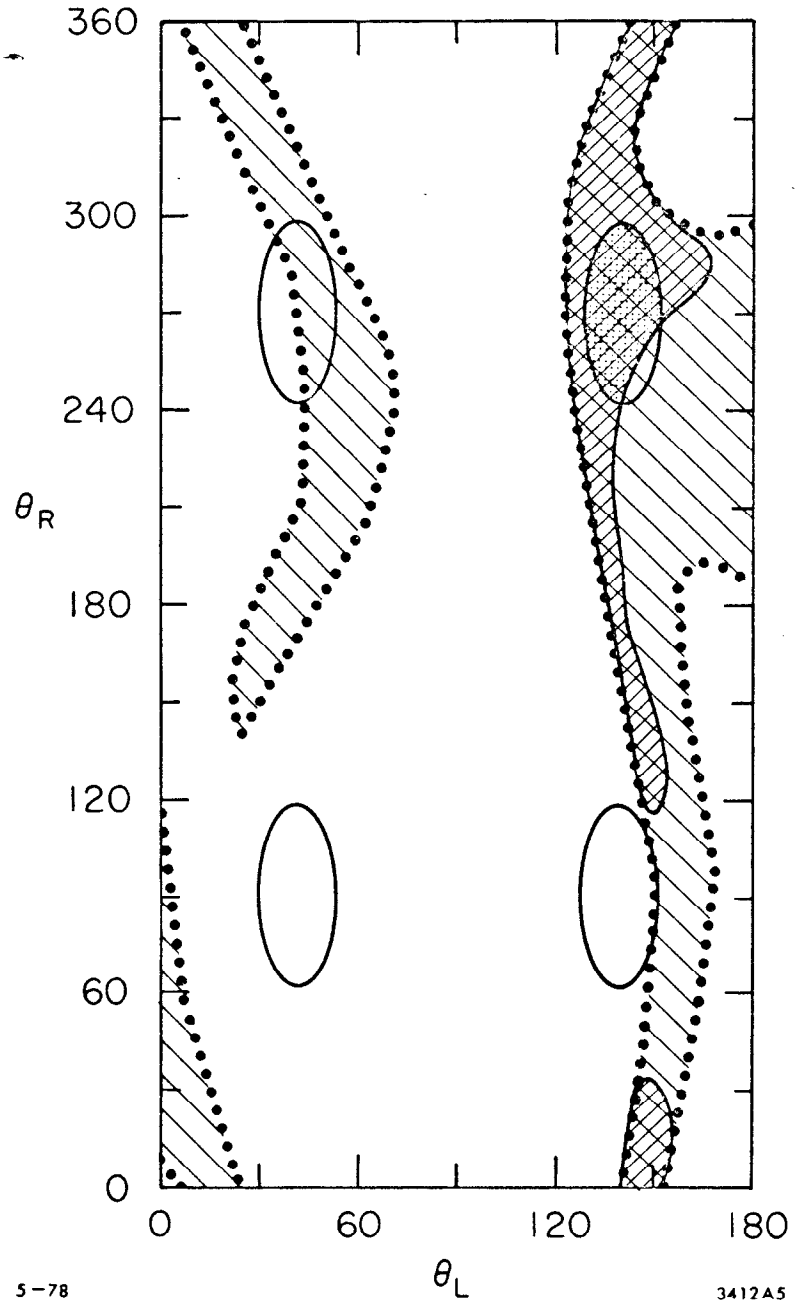

Fig. 2

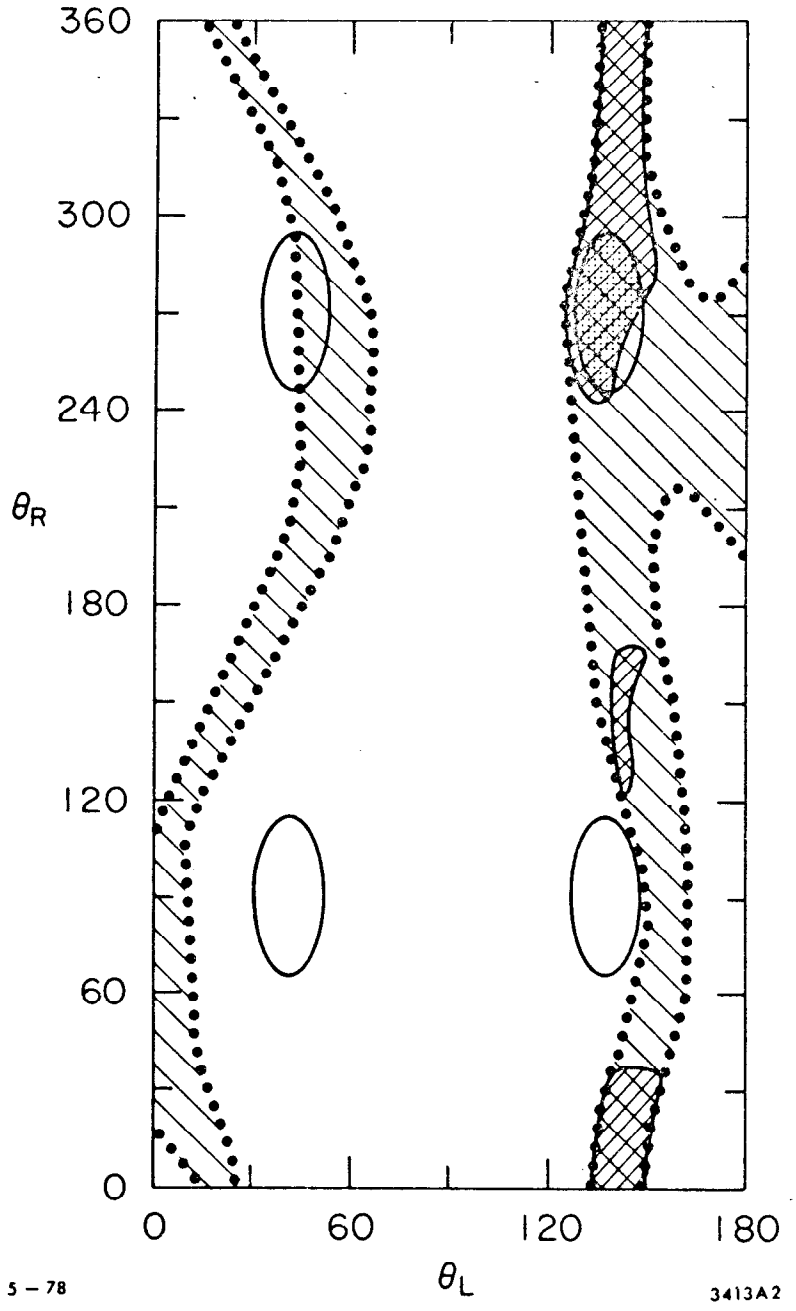

Fig. 3

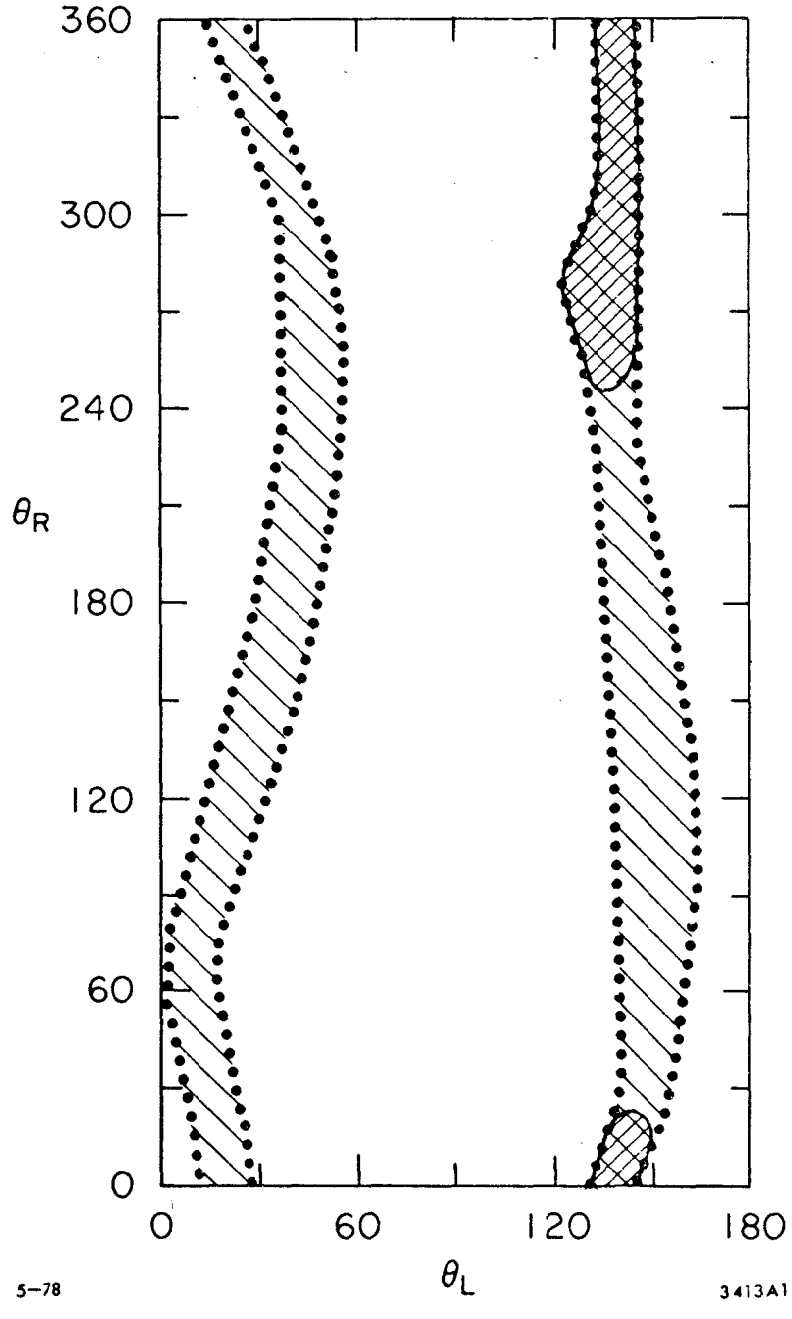

Fig. 4

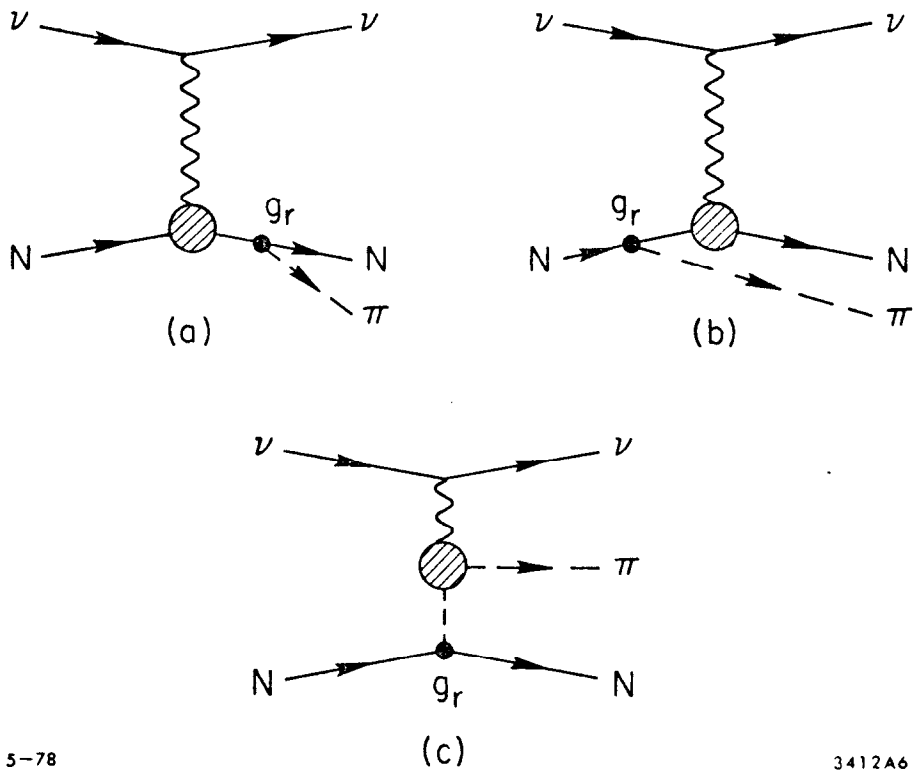

Fig. 5

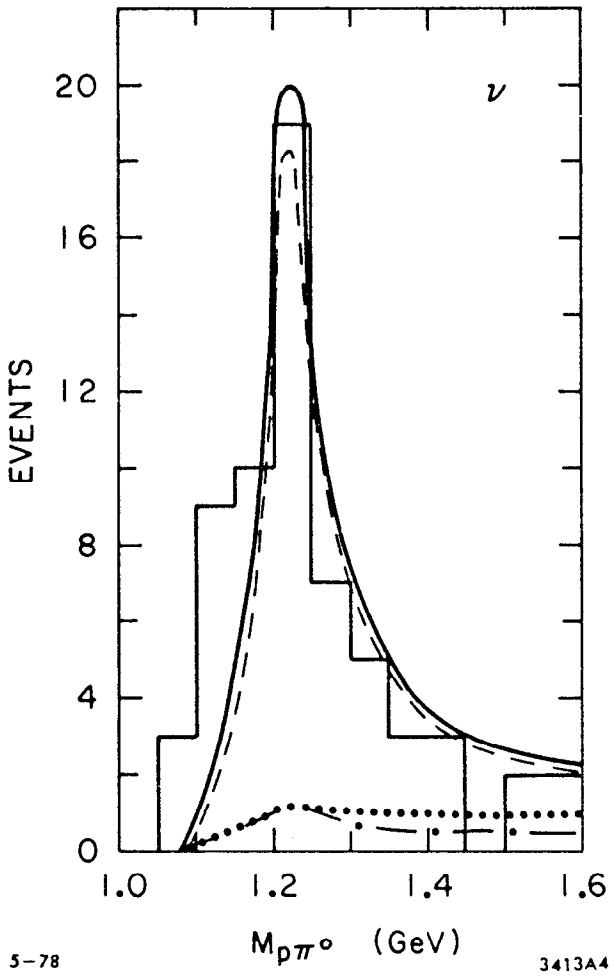

Fig. 6

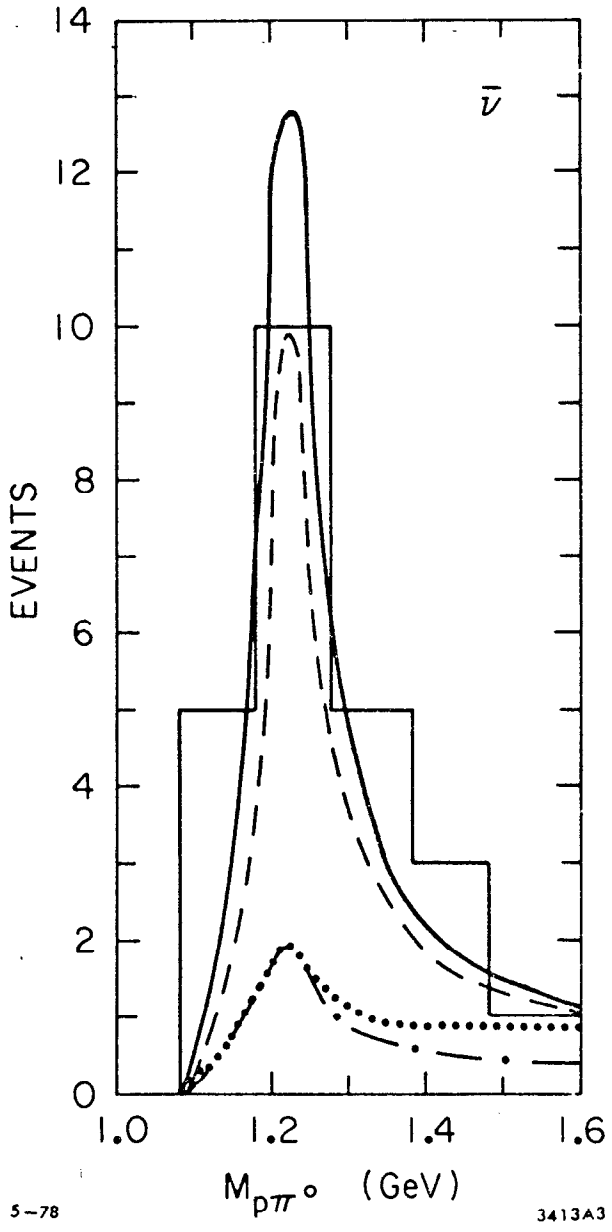

Fig. 7

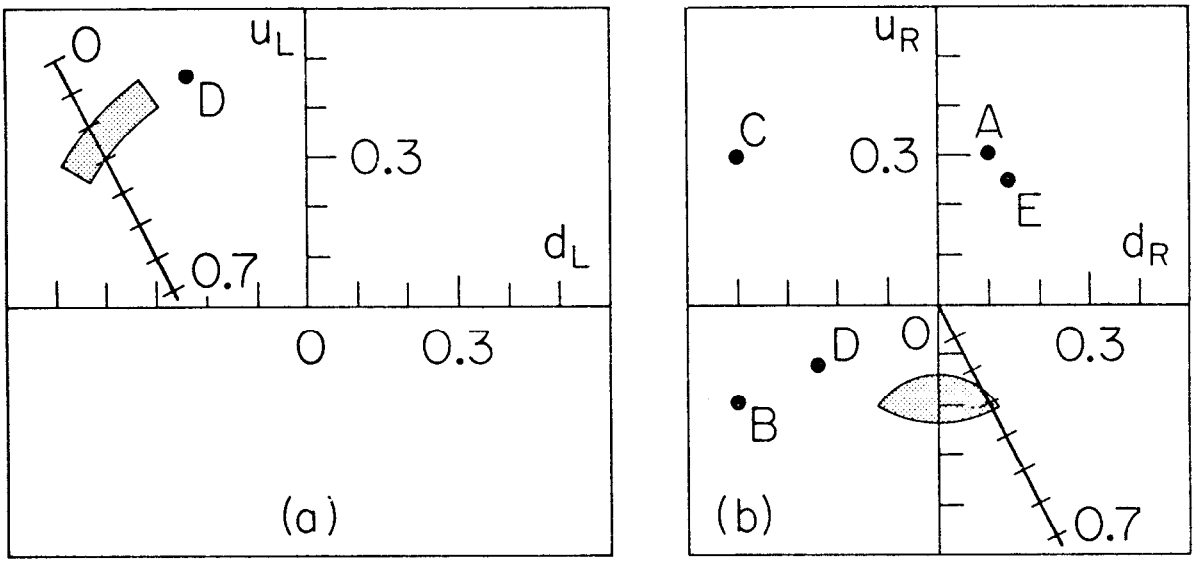

5 – 78

3366A2

Fig. 8

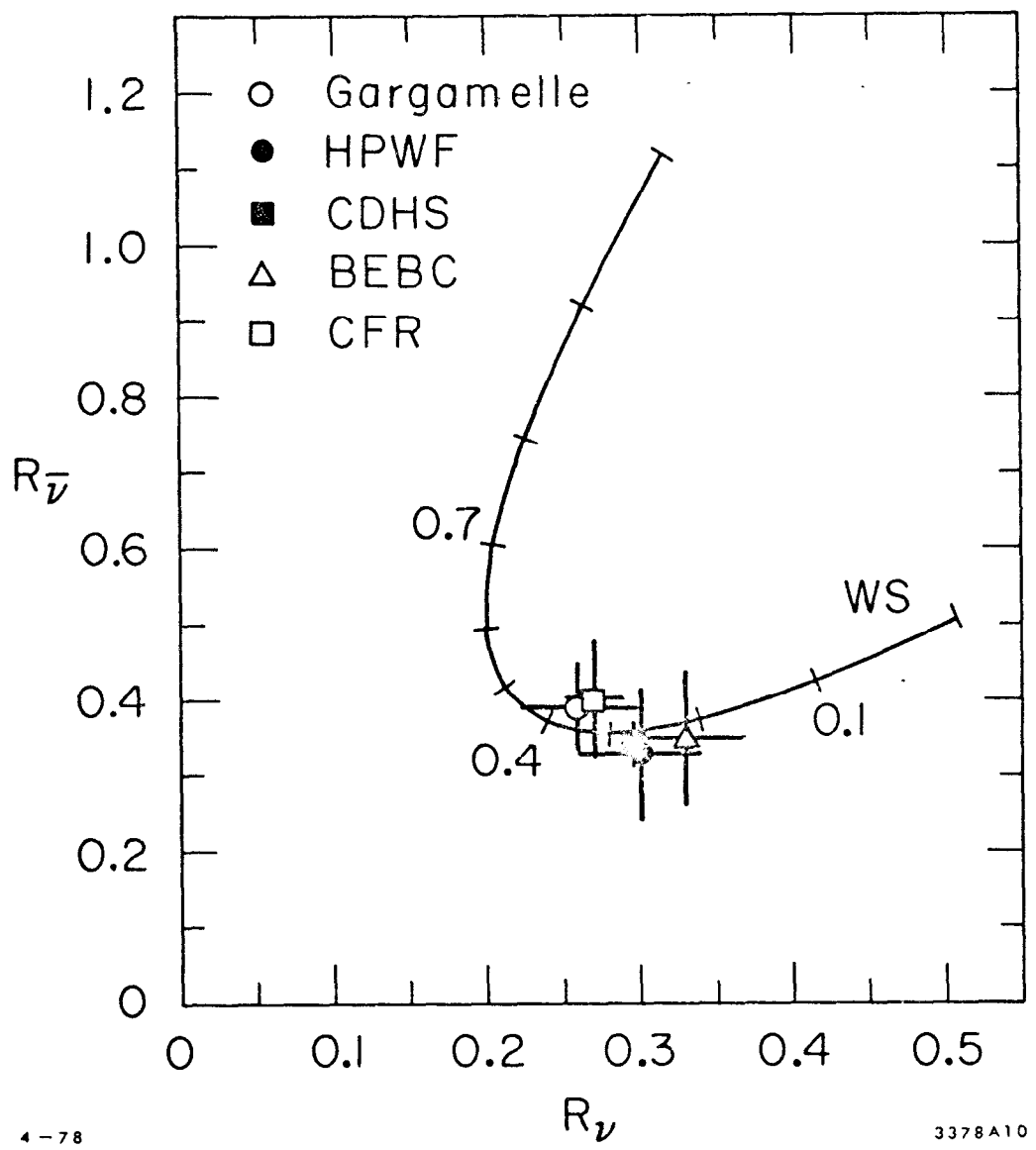
Gargamelle
HPWF
CDHS
BEBC
CFR
1.2
1.0
0.8
0.6
0.4
0.2
0
$R_{\bar{\nu}}$
0.7
WS
0.1
0.4
0
0.1
0.2
0.3
0.4
0.5
R_{ν}
4-78
3378A10

Fig. 9

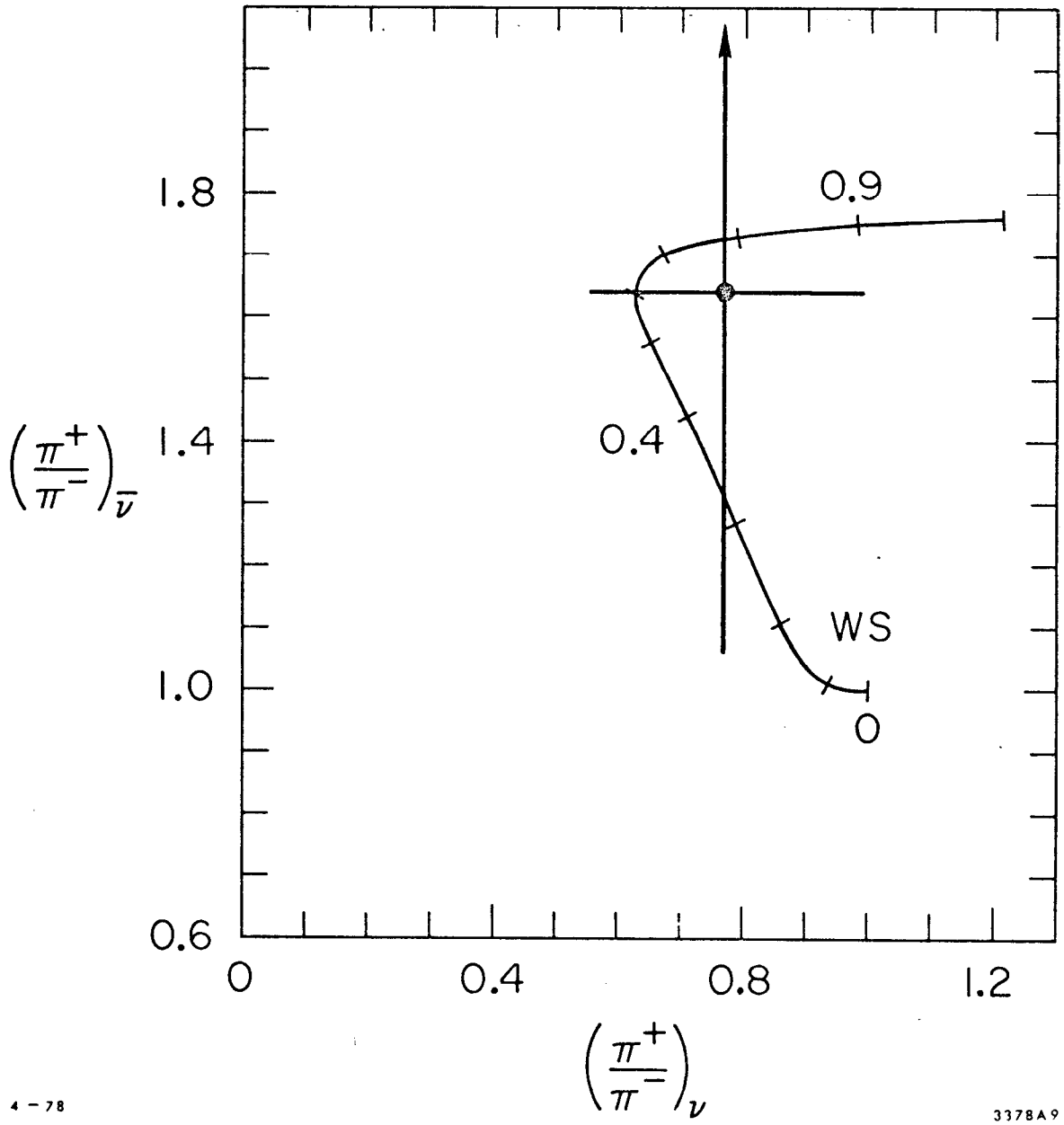

4 – 78

3378A9

Fig. 10

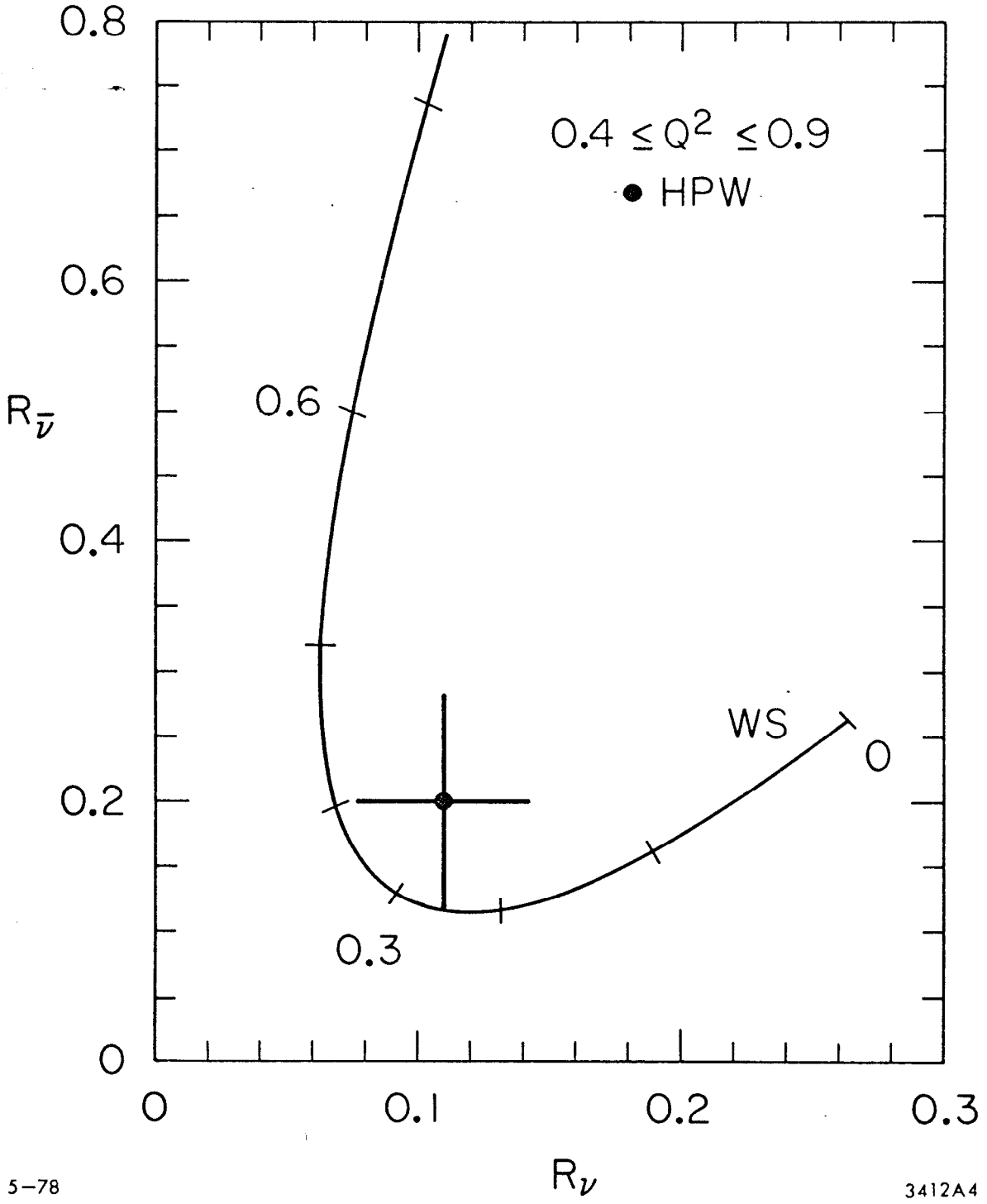
0.8
0.6
0.4
0.2
0
$R_{\bar{\nu}}$
$0.4 \leq Q^2 \leq 0.9$
HPW
0.6
WS
0
0.3
0
0.1
0.2
0.3
R_ν
5–78
3412A4

Fig. 11

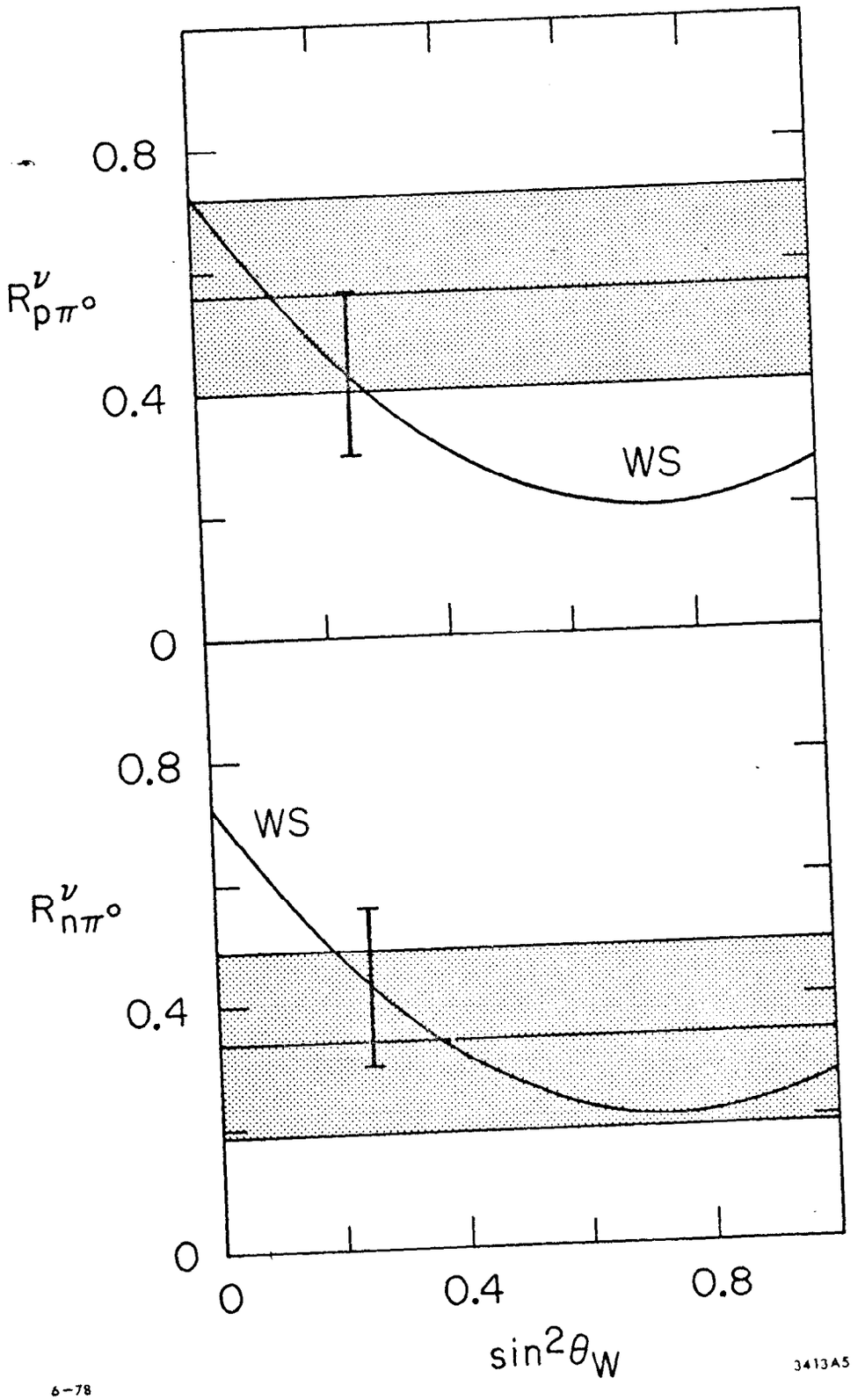
0.8
$R^{\nu}_{p\pi^0}$
0.4
WS
0
0.8
WS
$R^{\nu}_{n\pi^0}$
0.4
0
0
0.4
0.8
$\sin^2\theta_W$
3413A5
6-78

Fig. 12

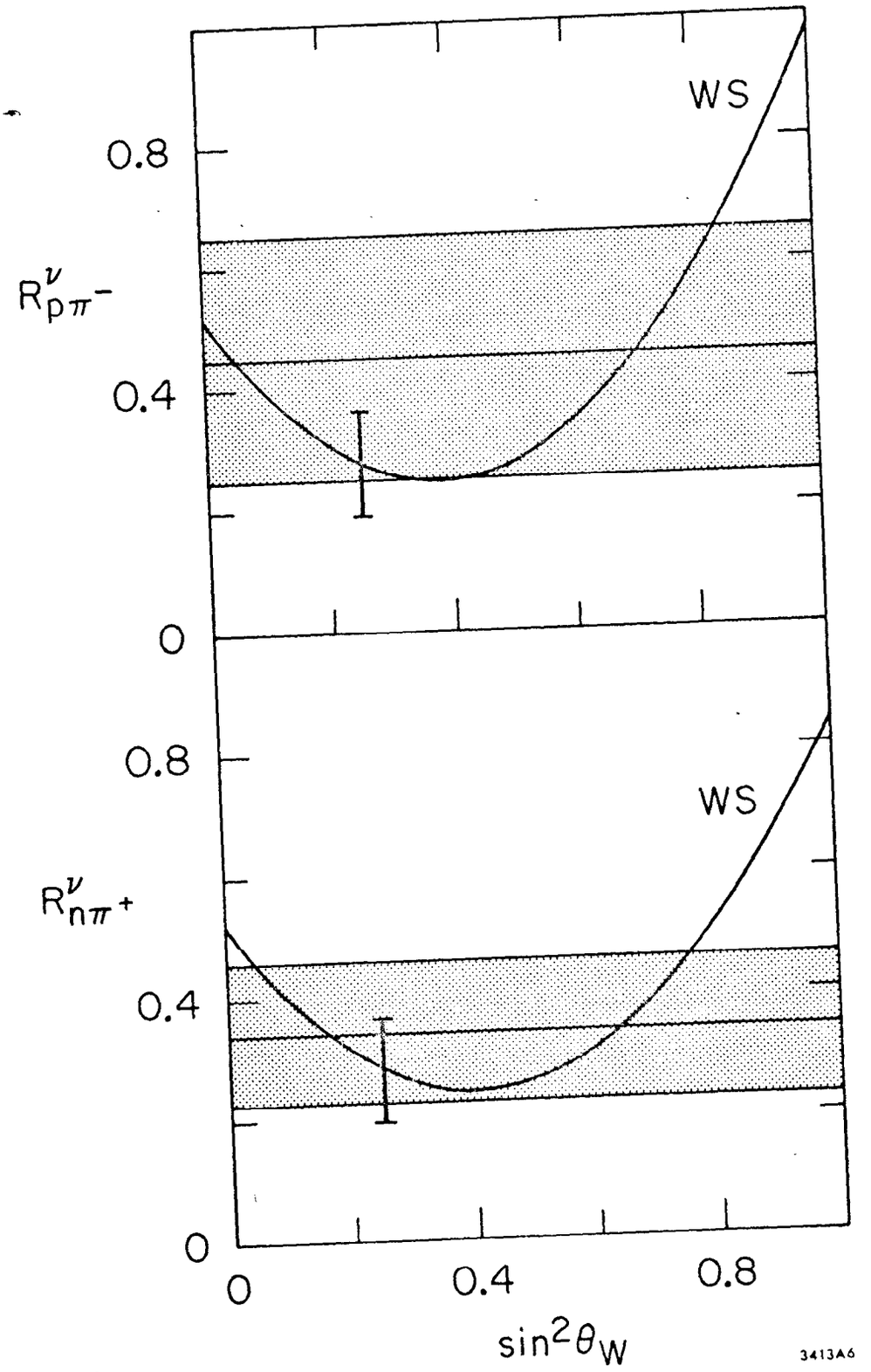

6-78

Fig. 13

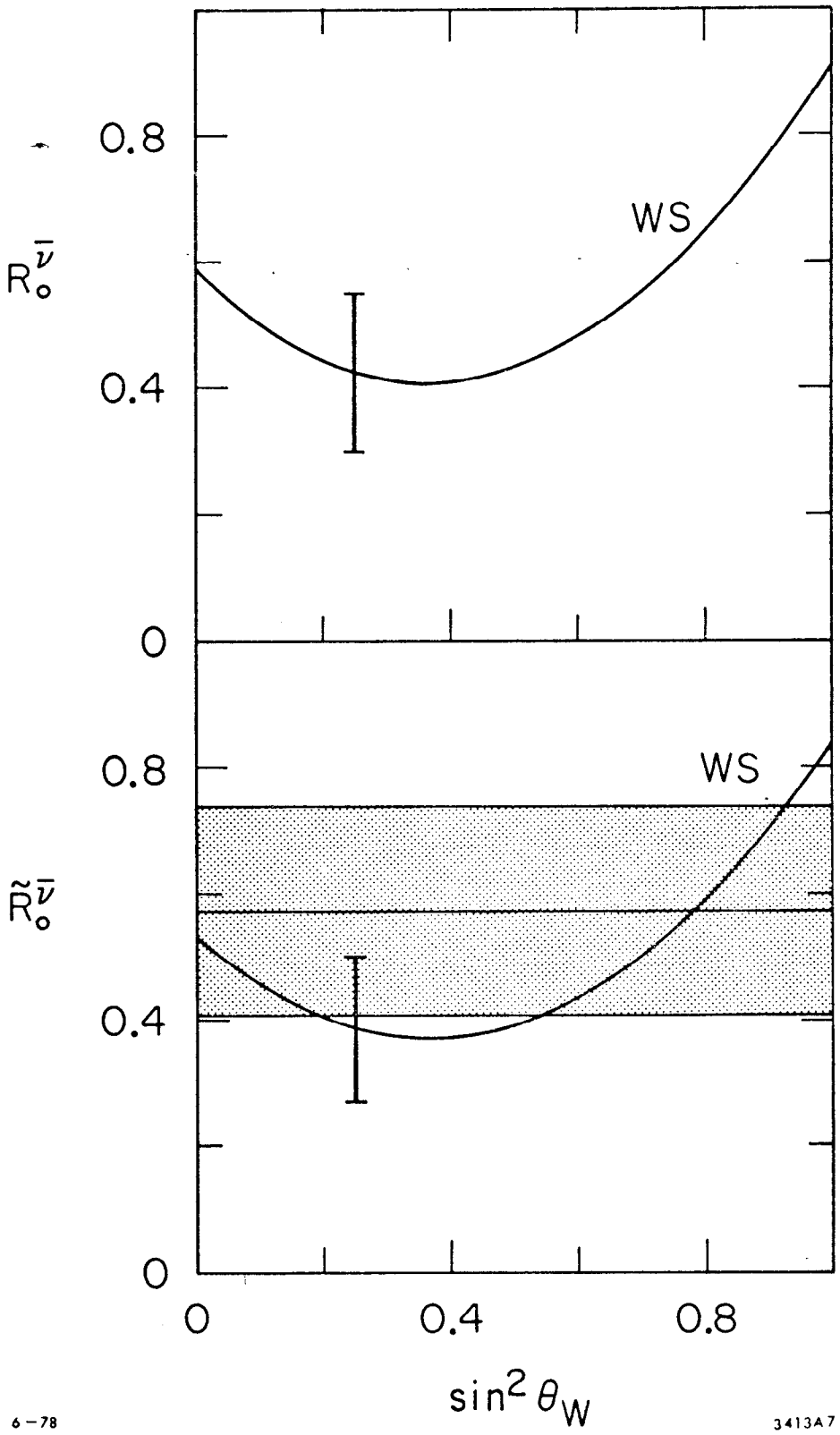
0.8
0.4
0
$R_o^{\bar{\nu}}$
WS
0.8
0.4
0
$\tilde{R}_o^{\bar{\nu}}$
WS
0
0.4
0.8
$\sin^2\theta_W$
6-78
3413A7

Fig. 14

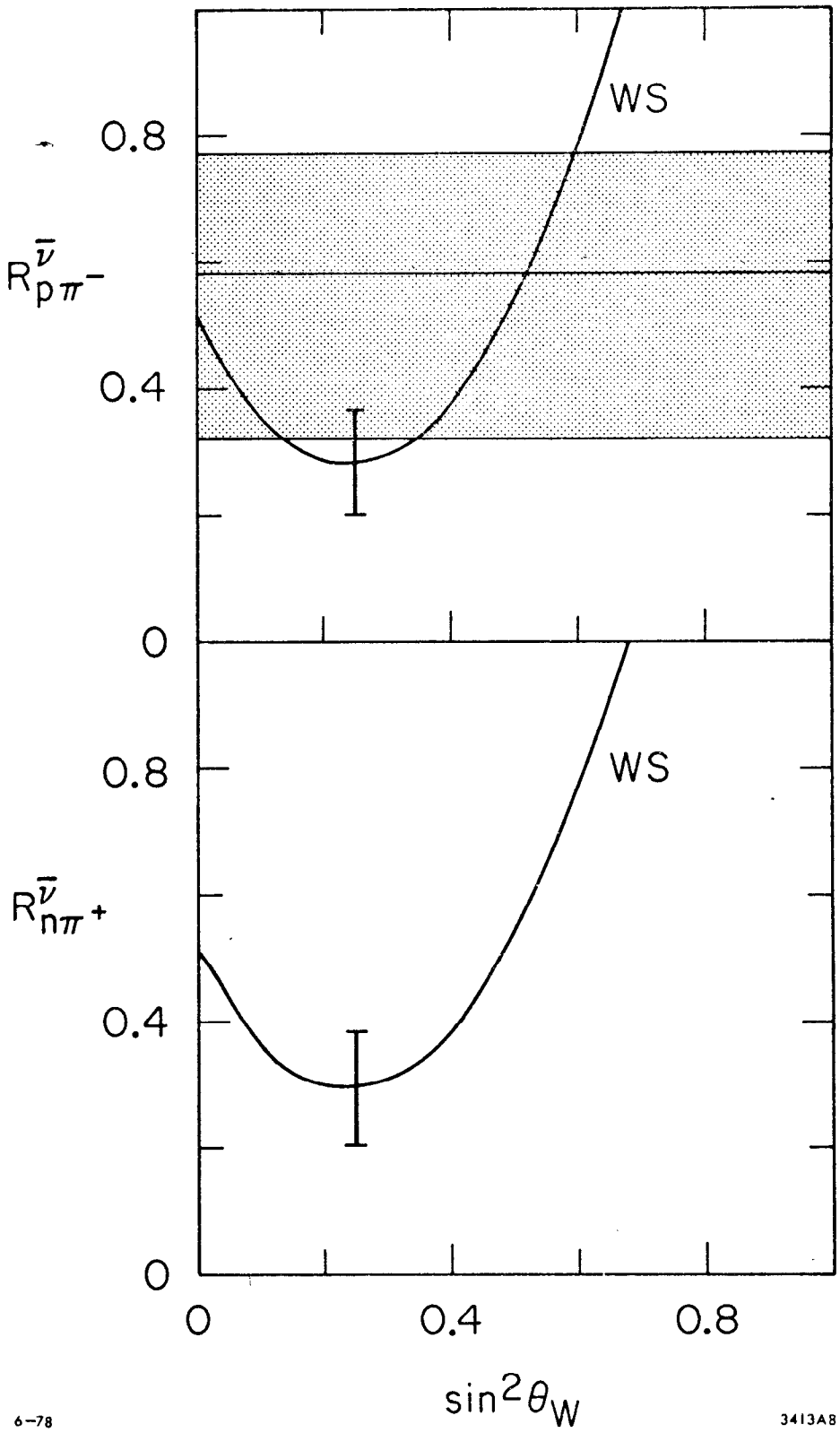
WS
0.8
$R^{\bar{\nu}}_{p\pi^-}$
0.4
0
WS
0.8
$R^{\bar{\nu}}_{n\pi^+}$
0.4
0
0
0.4
0.8
$\sin^2\theta_W$
6-78
3413A8

Fig. 15

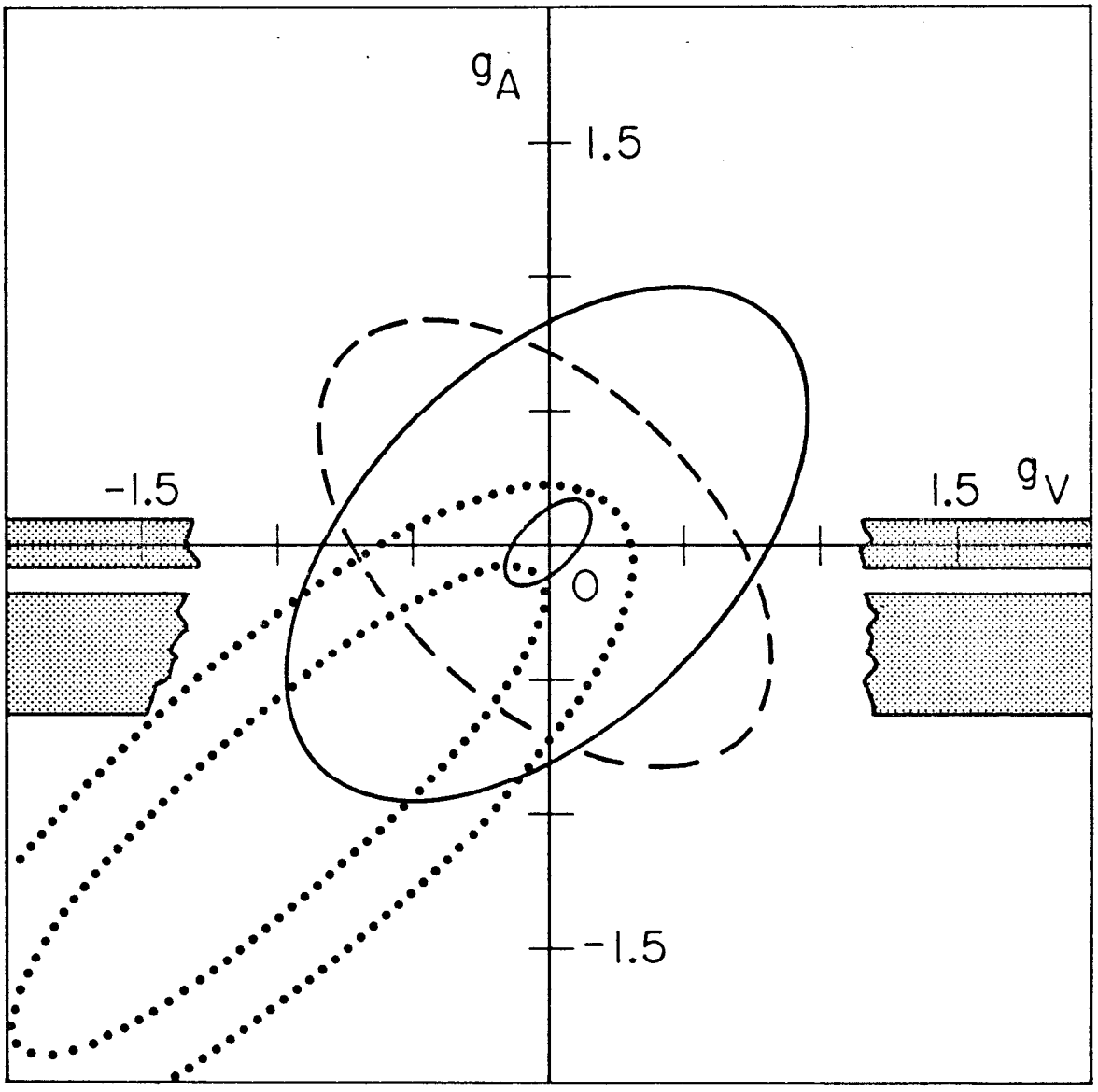

6 — 78

3413A9

Fig. 16

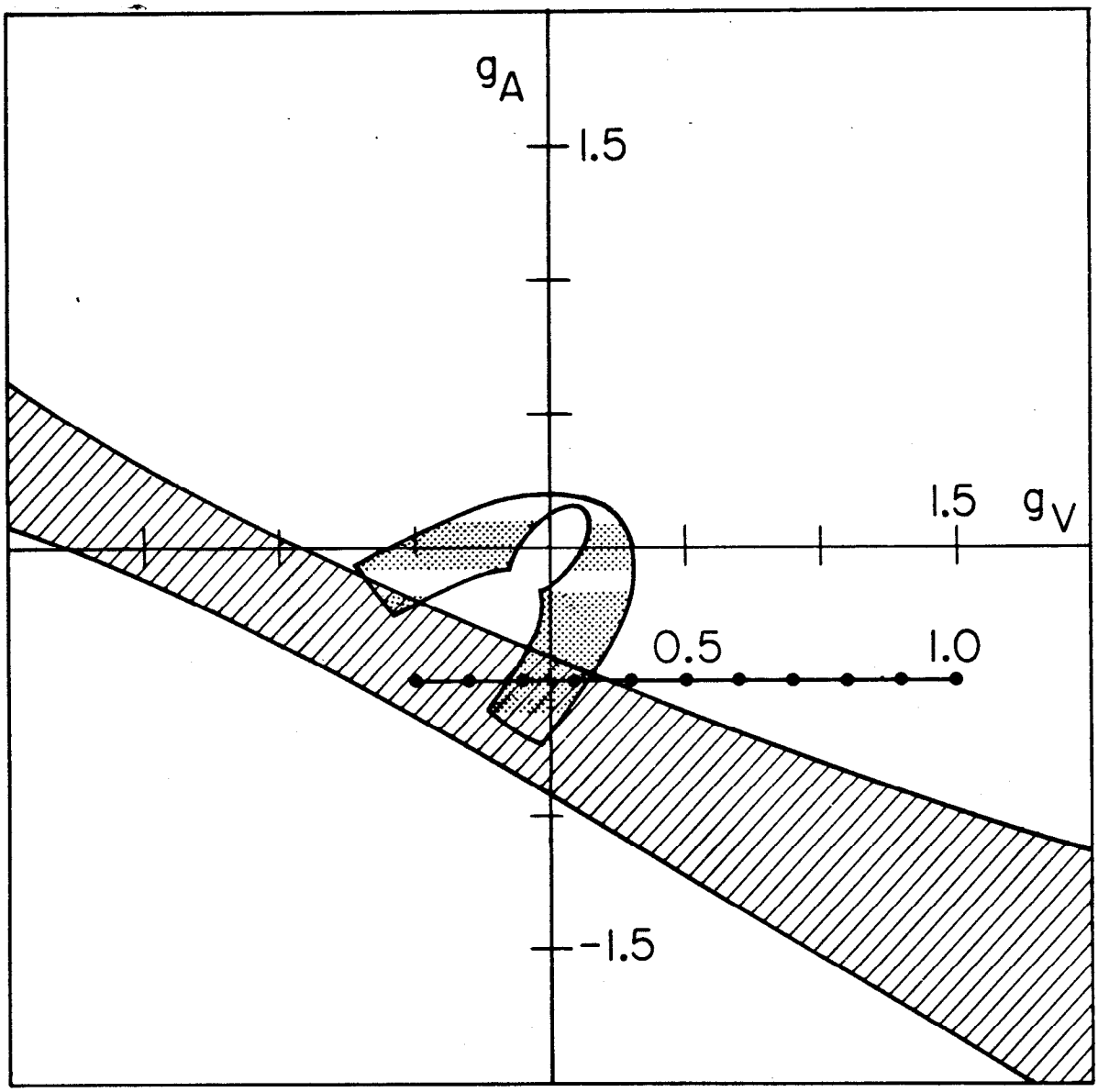

Fig. 17

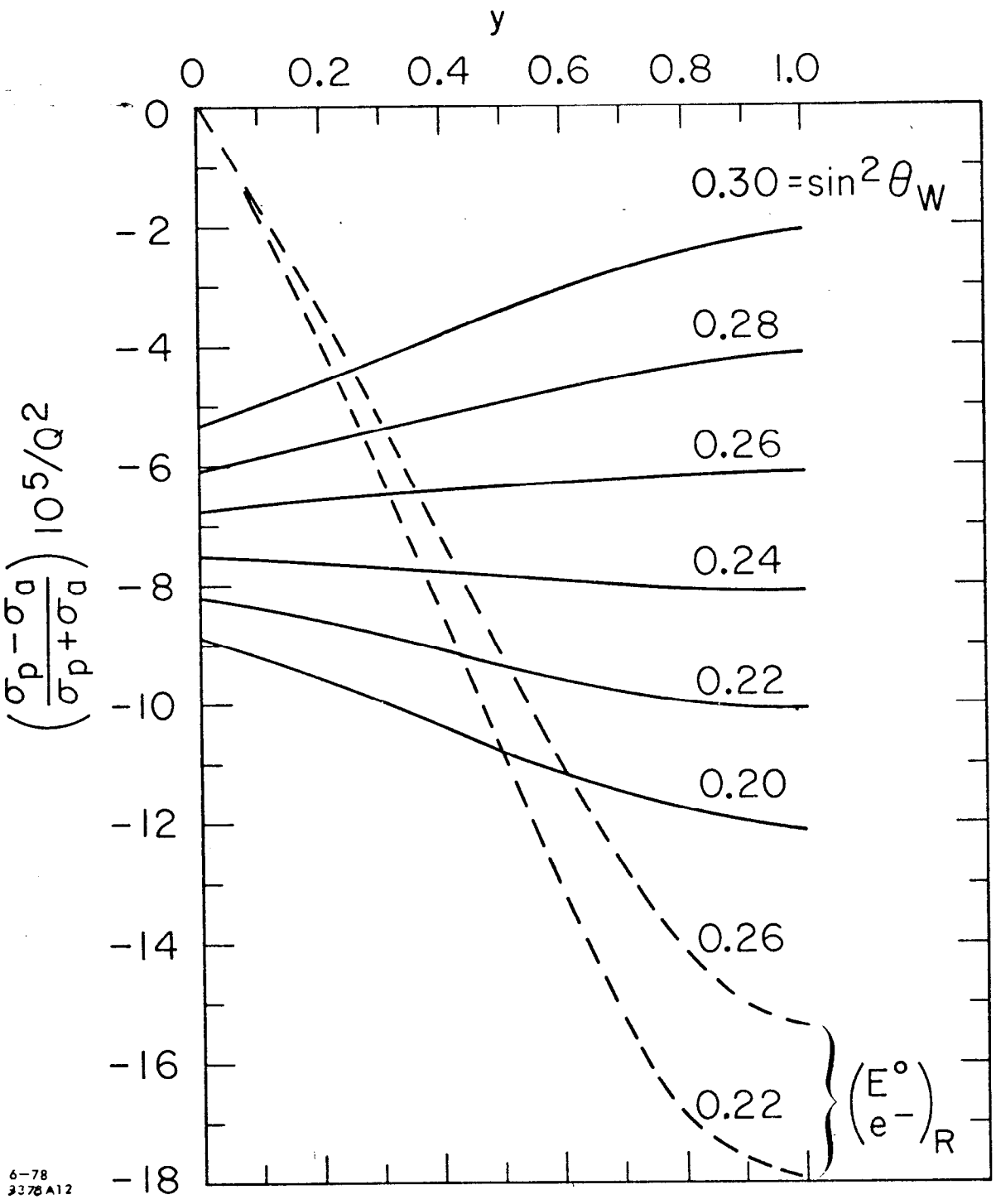
y
0
0.2
0.4
0.6
0.8
1.0
0
-2
-4
-6
-8
-10
-12
-14
-16
-18
$\left(\frac{\sigma_p-\sigma_a}{\sigma_p+\sigma_a}\right) 10^5/Q^2$
$0.30=\sin^2\theta_W$
0.28
0.26
0.24
0.22
0.20
0.26
0.22
$\left(\begin{matrix}E^\circ\\ e-\end{matrix}\right)_R$
6-78
3378A12

Fig. 18